The Supporting Information was updated on 16th May 2019

Supporting Information

Heterodinuclear Zinc and Magnesium Catalysts for Epoxide/CO_2 Ring Opening Copolymerisations

G. Trott[1], J. A. Garden[2] and C. K. Williams[1]*

[1]*Chemistry Research Laboratory, University of Oxford, Mansfield Road, Oxford, OX1 3TA, UK*

[2] *School of Chemistry, University of Edinburgh, EH9 3FJ, UK.*

Contents

1. Experimental Section

Materials

All metal complexes were synthesised under anhydrous conditions, using standard glovebox and Schlenk line techniques. The macrocyclic ligand was synthesised according to literature procedures.[1] All solvents used were dried, degassed by at least three freeze-pump-thaw cycles and stored over activated 4 Å molecular sieves under nitrogen. Research grade carbon dioxide (BOC, 99.99 %) was used for all copolymerisation studies and dried through two MicroTorr purifier columns at point of use, with a flow rate below 0.5 slpm (standard litre per minute).

Cyclohexene oxide was dried over calcium hydride and fractionally distilled under nitrogen at atmospheric pressure. Cyclopentene oxide was dried over calcium hydride and then a vacuum transfer was carried out, before drying it with sodium hydride and collecting it via vacuum transfer. The epoxides were stored under nitrogen.

Low pressure Copolymerisations

For polymerisations at 1 bar, a solution of catalyst (0.015 mmol) in epoxide (14.9 mmol) was added to a Schlenk tube in the glovebox. This Schlenk tube was then subjected to five rapid vacuum/CO_2 (pressure regulated to 1 bar) cycles, before the reaction was started by heating to 80 °C (unless the temperature was otherwise stated) in an oil bath. Aliquots were taken under a positive pressure of CO_2. Reactions were quenched by cooling the sample and exposing it to air. ^{1}H NMR spectra were taken, in air and in $CDCl_3$, before the crude product was obtained through removal of volatile CHO under vacuum. SEC analysis was carried out on the crude sample which was re-dissolved in THF for analysis. When using i*n situ* ATR-IR spectroscopy to monitor reactions at low pressures, the Schlenk tube was fitted with a DiComp probe under a positive pressure of CO_2, before the reaction was started.

The procedure for monitoring diluted reactions was unchanged, except for the volumes used. When carrying out a series of kinetic investigations, the catalyst (0.05-0.2 mol%) was dissolved in CHO (2.5 mL) and diethyl carbonate (DEC) (0.5 mL).

High pressure CO_2/CHO Copolymerisation

For polymerisations at elevated pressures, a solution of catalyst (0.01-0.005 mol%) in epoxide (60 mmol) was added to the high pressure reactor, under N_2, in a glovebox. The reactor was secured before removing from the glovebox and then pressurised with CO_2 whilst heating to the desired temperature. The system was closed to further gas pressure for the duration of the polymerisation reaction. Reactions were quenched by cooling, depressurising and opening to air and the polymer samples analysed as before.

Potassium Salt Synthesis

Potassium benzoate and potassium acetate were obtained from commercial sources and dried overnight under vacuum before use. All other salts were synthesised trivially as below.

KOBz^{OMe}

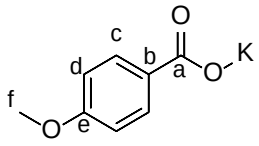

KH (320 mg, 7.98 mmol) was added to a Schlenk before the addition of dry THF (40 mL) and cooled to 0 °C. *p*-Anisic acid (1.24 g, 7.8 mmol) was slowly added via a solid addition tube and stirred for 15 min at 0 °C. The suspension was warmed to room temperature, stirred for 1 h and then the solvent filtered before drying the solid *in vacuo* to give the product as a white powder (1.25 g, 6.5 mmol, 82 % yield). ^{1}H NMR (400 MHz, d$_4$-methanol, δ(ppm)): 7.90 (d, 2H, $^{3}J_{H–H}$ = 9 Hz, c), 6.87 (d, 2H, $^{3}J_{H-H}$ = 9 Hz, d), 4.87 (s, 3H, f). ^{13}C{^{1}H} NMR (100 MHz, d$_4$-methanol, δ(ppm)): 175.4 (a), 163.0 (e), 132.1 (c), 131.5 (b), 113.8 (d), 55.7 (f). Calc. for $C_8H_7O_3K$: C, 50.51; H, 3.71; Found: C, 50.35; H, 3.90 %.

KOBz^{CF3}

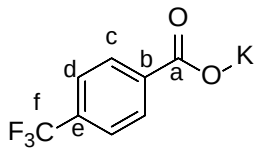

KH (320 mg, 7.98 mmol) was added to a Schlenk before the addition of dry THF (40 mL) and cooled to 0 °C. 4-(Trifluoromethyl)benzoic acid (1.52 g, 7.8 mmol) was slowly added via a solid addition tube and stirred, for 15 min, at 0 °C. The suspension was warmed to room temperature, stirred for 1 h, and then the solvent filtered off before drying the solid *in vacuo* to give the product as a white powder (1.47 g, 6.5 mmol, 81 % yield). ^{1}H NMR (400 MHz, d$_4$-methanol, δ(ppm)): 8.07 (d, 2H, $^{3}J_{H–H}$ = 8 Hz, c), 7.65 (d, 2H, $^{3}J_{H-H}$ = 8 Hz, d). ^{13}C{^{1}H} NMR (100 MHz, d$_4$-methanol, δ(ppm)): 173.6 (a), 143.2 (b), 132.7 (q, $^{2}J_{F–H}$ = 32 Hz, e), 130.7 (c), 125.8 (q, $^{1}J_{F–H}$ = 272 Hz, f), 125.7 (q, $^{3}J_{F–H}$ = 5 Hz, d). ^{19}F{^{1}H} NMR (376 MHz, d$_4$-methanol, δ(ppm)): -64.9 (s). Calc. for $C_8H_4F_3O_2K$: C, 42.10; H, 1.77; Found: C, 42.02; H, 1.74 %.

KOBz$^{NO2\ 2}$

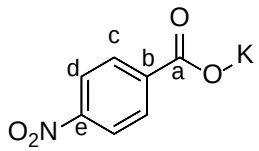

4-Nitrobenzoic acid (3.34 g, 20 mmol) was stirred in a round bottom flask in EtOH (30 mL) with a dropping funnel attached, containing KO^{t}Bu (2.24 g, 20 mmol) dissolved in EtOH (20 mL). This solution was added to the acid, dropwise over 1 hour, at room temperature and stirred for a further hour. The resulting solid was collected by filtration and washed with EtOH (2 x 10 mL) and cold Et$_2$O (10 mL). The product was collected as a white powder and dried *in vacuo* (2.17 g, 10.6 mmol, 53 % yield). ^{1}H NMR (400 MHz, d$_4$-methanol, δ(ppm)): 8.22 (d,

2H, $^{3}J_{H–H}$ = 9 Hz, d), 8.11 (d, 2H, $^{3}J_{H-H}$ = 9 Hz, c). $^{13}C\{^{1}H\}$NMR (100 MHz, d_4-methanol, δ(ppm)): 172.5 (a), 150.4 (e), 145.2 (b), 131.2 (c), 123.9 (d). Calc. for $C_7H_4NO_4K$: C, 40.97; H, 1.96; N, 6.83; Found: C, 41.09; H, 2.04; N, 6.76 %.

KOBz^{NMe2}

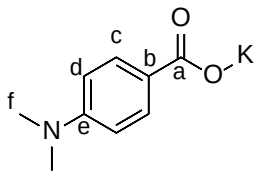

4-(Dimethylamino)benzoic acid (1.32 g, 8.0 mmol) was stirred in THF (40 mL) before the slow addition of $KN(SiMe_3)_2$ (1.59 g, 8.0 mmol). The suspension was stirred for 16 hours at room temperature before removal of the solvent by filtration. The resulting solid was washed with pentane and dried *in vacuo* to give the product as a white powder (1.51 g, 7.4 mmol, 93 % yield). ^{1}H NMR (400 MHz, d_4-methanol, δ(ppm)): 7.83 (d, 2H, $^{3}J_{H–H}$ = 9 Hz, c), 6.68 (d, 2H, $^{3}J_{H-H}$ = 9 Hz, d), 2.97 (s, 6H, f). $^{13}C\{^{1}H\}$ NMR (100 MHz, d_4-methanol, δ(ppm)): 176.4 (a), 153.7 (e), 131.8 (c), 126.3 (b), 112.3 (d), 40.5 (f). Calc. for $C_9H_{10}NO_2K$: C, 53.18; H, 4.96; N, 6.89; Found: C, 53.07; H, 5.01; N, 6.86 %.

KOBz^{F}

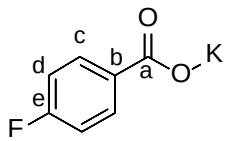

4-Fluorobenzoic acid (2.80 g, 20 mmol) was stirred in a round bottom flask in EtOH (20 mL) with a dropping funnel attached, containing KO^{t}Bu (2.24 g, 20 mmol) dissolved in EtOH (20 mL). This solution was added to the acid dropwise over 1 hour at room temperature and stirred for a further hour. The resulting solid was collected by filtration and washed with EtOH (2 x 10 mL) and cold Et_2O (10 mL). The product was collected as a white powder and dried *in vacuo* (3.25 g, 18.3 mmol, 91 % yield). ^{1}H NMR (400 MHz, d_4-methanol, δ(ppm)): 7.98 (m, 2H, c), 7.05 (m, 2H, d). $^{13}C\{^{1}H\}$ NMR (100 MHz, d_4-methanol, δ(ppm)): 174.2 (a), 165.6 (d, $^{1}J_{C–F}$ = 249 Hz, e), 135.5 (b), 132.6 (d, $^{3}J_{C–F}$ = 9 Hz, c), 115.2 (d, $^{2}J_{C–F}$ = 21 Hz, d). $^{19}F\{^{1}H\}$ NMR (376 MHz, d_4-methanol, δ(ppm)): -113.8. Calc. for $C_7H_4FO_2K$: C, 47.18; H, 2.26; Found: C, 47.30; H, 2.13 %.

KOBz^{F5} [2]

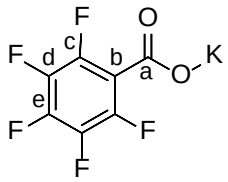

2,3,4,5,6-Pentafluorobenzoic acid (4.24 g, 20 mmol) was stirred in a round bottom flask in EtOH (20 mL) with a dropping funnel attached, containing KO^{t}Bu (2.24 g, 20 mmol) dissolved in EtOH (20 mL). This solution was added to the acid, dropwise over 1 hour, at room temperature and stirred for a further hour. The resulting solid was collected by filtration and washed with EtOH (2 x 10 mL) and cold Et_2O (10 mL). The product was collected as a white powder and dried *in vacuo* (4.32 g, 17.2 mmol, 86 % yield). $^{19}F\{^1H\}$ NMR (376 MHz, d_4-methanol, δ(ppm)): -145.4 (m, 2F, c), -161.0 (t, 1F, $^3J_{F-F}$ = 20 Hz, e), -165.4 (m, 2F, d). $^{13}C\{^1H\}$ NMR (100 MHz, d_4-methanol, δ(ppm)): 164.3 (a), 144.1 (doublet of multiplets, $^1J_{C-F}$ = 245 Hz, c/d), 141.5 (doublet of multiplets, $^1J_{C-F}$ = 250 Hz, e), 138.6 (doublet of multiplets, $^1J_{C-F}$ = 251 Hz, c/d), 118.4 (triplet of multiplets, $^2J_{C-F}$ = 25 Hz, b). Calc. for $C_7F_5O_2K$: C, 33.61; Found: C, 33.52 %.

Catalyst Synthesis

Synthesis of 1

LH_2 (1.0 g, 1.82 mmol) and THF (5 mL) were added to a Schlenk tube, before the addition of a solution of $ZnEt_2$ (224 mg, 1.82 mmol) in THF (5 mL). The reaction mixture was stirred for 16 hours, at room temperature, before the addition of more THF (10 mL). This solution was cooled to -78 °C whilst stirring and then a solution of $MgBr_2$ (334 mg, 1.82 mmol), in THF (20 mL) was added, dropwise, over 15 min. The reaction mixture was stirred at -78 °C, for 15 min, and then at room temperature, for 30 min, before the solvent was removed. The white powder was dried *in vacuo* overnight to yield the product (1.44 g, 1.80 mmol, 99 %). ^1H NMR (400 MHz, d_4-methanol, δ(ppm)): 7.05 (m, 2H, b'), 7.01(m, 2H, b), 4.91 (d, 2H, c), 4.10 (d, 2H, c'), 3.28 (d, 2H, d'), 3.23 (d, 2H, d), 3.07 (d, 2H, e), 2.75 (d, 2H, e'), 2.64 (d, 2H, f), 2.62 (d, 2H, f'), 1.25 (s, 18H, a), 1.08 (s, 3H, g), 1.06 (s, 3H, g'), 1.00 (s, 3H, h), 0.98 (s, 3H, h'). $^{13}C\{^1H\}$ NMR (100 MHz, d_4-methanol, δ(ppm)): 161.5 (f), 139.1 (c), 129.4 (d'), 129.0 (d), 125.5 (e'), 124.7 (e), 64.0 (h), 63.4 (h'), 58.2 (g), 56.4 (g'), 35.0 (i'), 34.4 (b), 34.3 (i), 32.0 (a), 28.6 (j'), 28.3 (j), 21.6 (k), 21.0 (k'). Calc. for $C_{34}H_{54}O_2N_4MgZnBr_2$: C, 51.03; H, 6.80; N, 7.00; Found: C, 51.23; H, 6.84; N, 6.94 %.

General procedure for synthesis of carboxylate-based catalysts

The intermediate complex, **1**, was synthesised as above, on a 0.91 mmol scale, without extensive drying. After complex formation in solution, the solvent was removed, the sample taken into the glovebox and the corresponding KX salt (1.82 mmol) was then added and stirred for 16 hours at room temperature. The resulting solid (KBr) was removed by filtration and the solution concentrated before the addition of DCM (2 mL). The solution was stirred for 1 hour before being filtered again and dried *in vacuo* to give the desired complex.

Where the scale of the reaction was altered, all reagent and solvent quantities were scaled accordingly.

Characterisation of Complexes 2a-h

Complex 2a

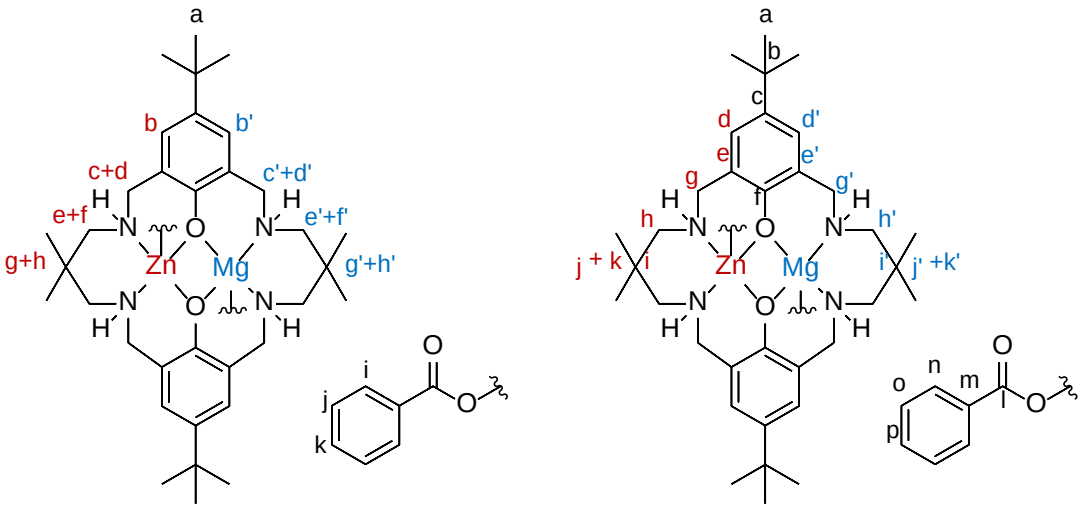

Synthesised on a 1.82 mmol scale. Yielded a white powder (1.53 g, 1.73 mmol, 95 %).

^{1}H NMR (400 MHz, d$_4$-methanol, δ(ppm)): 7.85 (br s, 4H, i), 7.33 (br t, $^{3}J_{H-H}$ = 6 Hz, 2H, k), 7.26 (br t, $^{3}J_{H-H}$ = 6 Hz, 4H, j), 6.96 (s, 4H, b+b'), 4.24 (d, $^{2}J_{H-H}$ = 12 Hz, 2H, c), 4.05 (d, $^{2}J_{H-H}$ = 12 Hz, 2H, c'), 3.27 (br m, 4H, d+d'), 2.91 (br d, $^{2}J_{H-H}$ = 11 Hz, 2H, e), 2.86-2.78 (m, 4H, f+e'), 2.71 (br d, $^{2}J_{H-H}$ = 11 Hz, 2H, f'), 1.43 (m, 6H, g+g'), 1.17 (s, 18H, a), 1.05 (m, 6H, h+h'). ^{13}C{^{1}H} NMR (100 MHz, d$_4$-methanol, δ(ppm)): 174.4 (l), 162.8 (f), 138.1 (c), 131.4 (p), 130.3 (n), 129.2 (d'), 129.1 (m), 129.0 (d), 128.5 (o), 125.3 (e'), 124.6 (e), 64.2 (h), 63.4 (h'), 56.9 (g), 56.2 (g'), 35.4 (i'), 34.9 (i), 34.3 (b), 32.0 (a), 28.9 (j'), 28.8 (j), 21.8 (k'), 21.3 (k). IR ($\nu_{c=o}$, cm^{-1}, neat): 1603 (a, terminal), 1564 (a, bridging), 1387 (s, terminal). MS (MALDI-ToF): m/z 758 [LMgZn(OBz)]$^{+}$ (100 %). Calc. for $C_{48}H_{64}O_6N_4MgZn$: C, 65.31; H, 7.31; N, 6.35; Found: C, 65.17; H, 7.43; N, 6.39 %.

Complex 2b

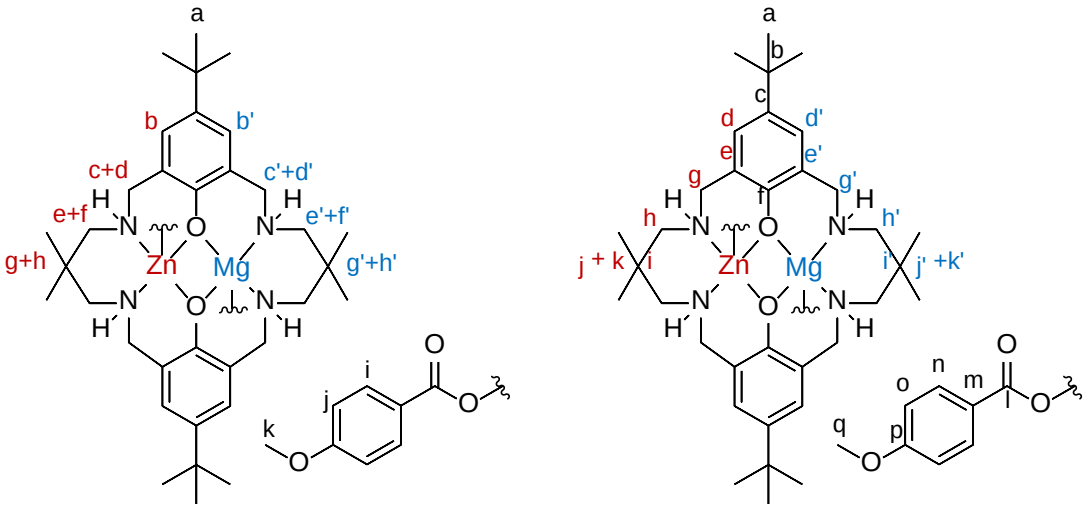

Synthesised on a 1.82 mmol scale. Yielded a white powder (1.40 g, 1.48 mmol, 82 %).

^{1}H NMR (400 MHz, d_4-methanol, δ(ppm)): 7.82 (br s, 4H, i), 6.96 (m, 4H, b+b'), 6.79 (br s, 4H, j), 4.23 (m, 2H, c), 4.09-4.02 (m, 2H, c'), 3.76 (s, 6H, k), 3.29-3.20 (m, 4H, d+d'), 2.91-2.87 (br m, 2H, e), 2.86-2.78 (m, 4H, f+e'), 2.70 (br d, 2H, f'), 1.44-1.41 (m, 6H, g+g'), 1.21-1.15 (m, 18H, a), 1.06-1.03 (m, 6H, h+h'). ^{13}C{^{1}H} NMR (100 MHz, d_4-methanol, δ(ppm)): 174.5 (l), 163.1 (p), 162.8 (f), 138.1 (c), 132.2 (n), 129.3 (d'), 129.0 (d), 128.1 (m), 125.3 (e'), 124.6 (e), 113.7 (o), 64.3 (h), 63.4 (h'), 56.9 (g), 56.3 (g'), 55.7 (q), 35.4 (i'), 34.8 (i), 34.3 (b), 32.0 (a), 28.9 (j'), 28.8 (j), 21.9 (k'), 21.3 (k). IR ($\nu_{c=o}$, cm^{-1}, neat): 1597 (a, terminal), 1558 (a, bridging), 1381 (s, terminal). MS (MALDI-ToF): m/z 790 [LMgZn(OBz^{OMe})]$^{+}$ (100 %). Calc. for $C_{50}H_{68}O_8N_4MgZn$: C, 63.70; H, 7.27; N, 5.94; Found: C, 63.51; H, 7.18; N, 5.82 %.

Complex 2c

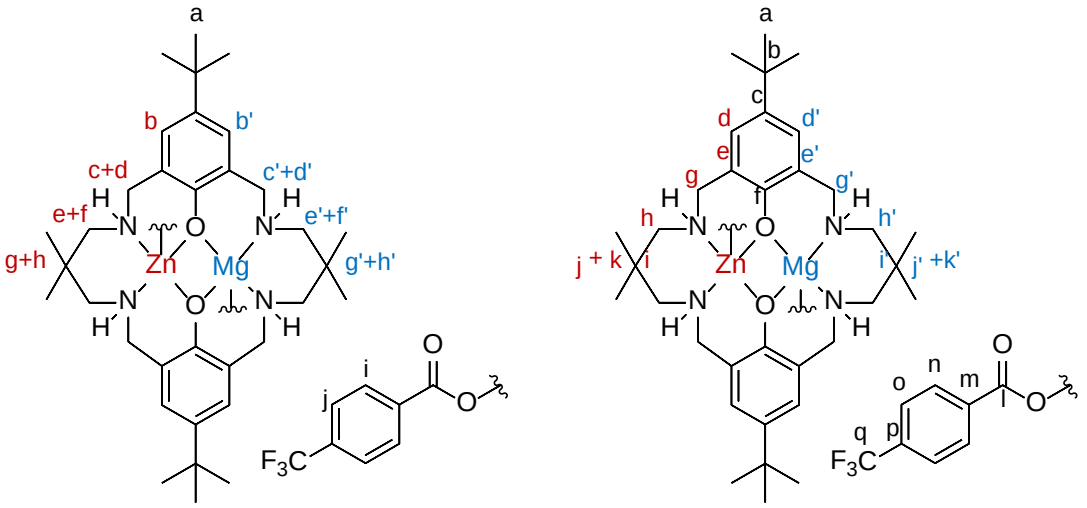

Synthesised on a 0.91 mmol scale. Yielded a white powder (780 mg, 0.71 mmol, 78 %).

^{1}H NMR (400 MHz, d_4-methanol, δ(ppm)): 8.01 (br s, 4H, i), 7.58 (br d, $^{3}J_{H-H}$ = 7 Hz, 4H, j), 6.96 (s, 4H, b+b'), 4.24 (d, $^{2}J_{H-H}$ = 12 Hz, 2H, c), 4.06 (d, $^{2}J_{H-H}$ = 12 Hz, 2H, c'), 3.30 (br d,

$^{2}J_{H-H}$ = 12 Hz, 2H, d), 3.22 (br t, $^{2}J_{H-H}$ = 12 Hz, 2H, d'), 2.91 (br d, $^{2}J_{H-H}$ = 12 Hz, 2H, e), 2.86-2.78 (m, 4H, f+e'), 2.71 (br d, $^{2}J_{H-H}$ = 12 Hz, 2H, f'), 1.42 (s, 6H, g+g'), 1.16 (s, 18H, a), 1.06 (s, 6H, h+h'). $^{13}C\{^{1}H\}$ NMR (100 MHz, d_4-methanol, δ(ppm)): 172.9 (l), 162.8 (f), 138.1 (c), 132.8 (q, $^{2}J_{C-F}$ = 32 Hz, p), 130.8 (n), 129.3 (d'), 129.1 (m), 129.0 (d), 125.7 (q, $^{1}J_{C-F}$ = 270 Hz, q), 125.6 (q, $^{3}J_{C-F}$ = 3 Hz, o), 125.4 (e'), 124.6 (e), 64.2 (h), 63.4 (h'), 56.9 (g), 56.2 (g'), 35.4 (i'), 34.9 (i), 34.3 (b), 32.0 (a), 28.9 (j'), 28.8 (j), 21.8 (k'), 21.4 (k). $^{19}F\{^{1}H\}$ NMR (377 MHz, d_4-methanol, δ(ppm)): -62.8 (s). IR ($\nu_{c=o}$, cm^{-1}, neat): 1618 (a, terminal), 1566 (a, bridging), 1391 (s, terminal). MS (MALDI-ToF): m/z 827 $[LMgZn(OBz^{CF3})]^{+}$ (90 %). Calc. for $C_{50}H_{62}F_6O_6N_4MgZn$: C, 58.95; H, 6.13; N, 5.50; Found: C, 58.77; H, 6.31; N, 5.38 %.

Complex 2d

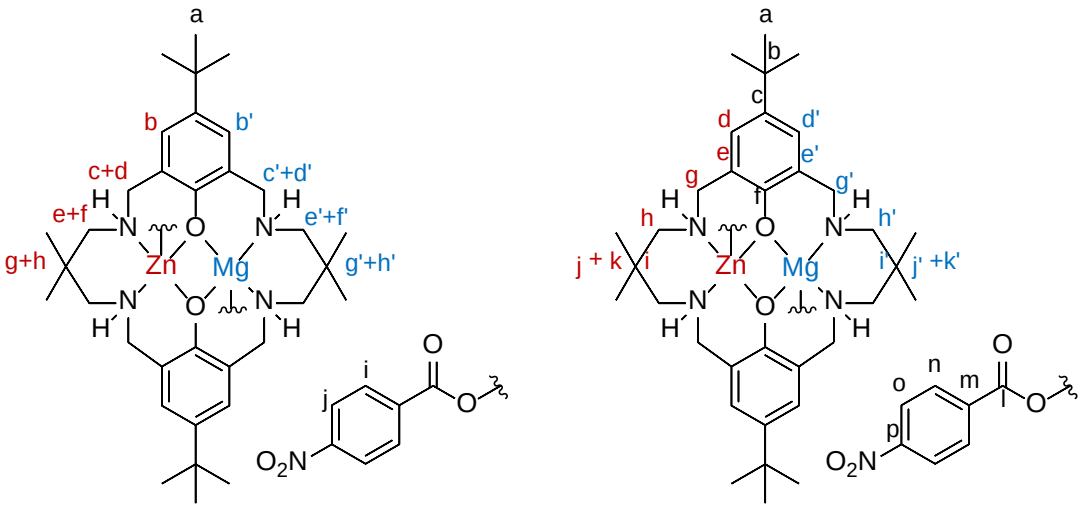

Synthesised on a 0.91 mmol scale. Yielded an orange powder (753 mg, 0.77 mmol, 85 %).

^{1}H NMR (400 MHz, d_4-methanol, δ(ppm)): 8.13 (br s, 4H, i), 8.05 (br s, 4H, j), 7.00-6.96 (m, 4H, b+b'), 4.25-4.17 (m, 2H, c), 4.08-4.01 (m, 2H, c'), 3.41-3.36 (m, 2H, d), 3.29-3.24 (m, 2H, d'), 2.98-2.88 (m, 2H, e), 2.86-2.77 (m, 4H, f+e'), 2.73-2.70 (m, 2H, f'), 1.42-1.40 (m, 6H, g+g'), 1.22-1.14 (m, 18H, a), 1.07-1.00 (m, 6H, h+h'). $^{13}C\{^{1}H\}$ NMR (100 MHz, d_4-methanol, δ(ppm)): 171.9 (l), 162.8 (f), 150.5 (p), 138.6 (m), 138.2 (c), 131.4 (o), 129.4 (d'), 129.2 (d), 125.4 (e'), 124.6 (e), 123.8 (n), 64.2 (h), 63.4 (h'), 56.9 (g), 56.3 (g'), 35.4 (i'), 34.8 (i), 34.3 (b), 32.0 (a), 28.9 (j'), 28.8 (j), 21.9 (k'), 21.4 (k). IR ($\nu_{c=o}$, cm^{-1}, neat): 1626 (a, terminal), 1587 (a, bridging), 1383 (s, terminal). MS (MALDI-ToF): m/z 803 $[LMgZn(OBz^{NO2})]^{+}$ (100 %). Calc. for $C_{48}H_{62}O_{10}N_6MgZn$: C, 59.27; H, 6.42; N, 8.64; Found: C, 59.19; H, 6.58; N, 8.49 %.

Complex 2e

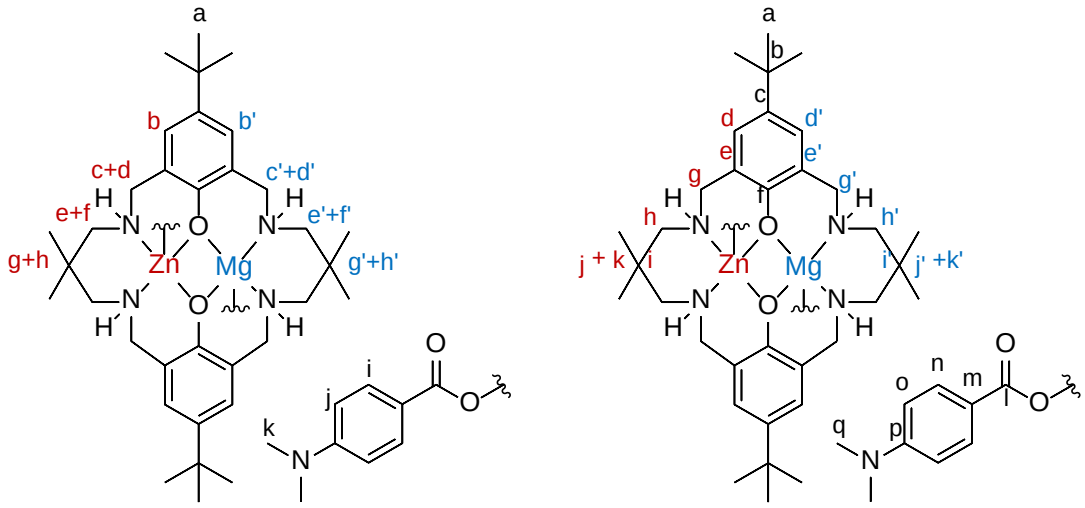

Synthesised on a 0.91 mmol scale. Yielded a white powder (0.484 g, 0.50 mmol, 55 %).

^{1}H NMR (400 MHz, d_4-methanol, δ(ppm)): 7.81 (br s, 4H, i), 6.96 (s, 4H, b+b'), 6.63 (br s, 4H, j), 4.22 (d, $^{2}J_{H-H}$ = 12 Hz, 2H, c), 4.04 (m, 2H, c'), 3.29-3.23 (br m, 4H, d+d'), 2.95 (s, 6H, k), 2.89 (br d, 2H, e), 2.85-2.75 (m, 4H, f+e'), 2.71 (br d, 2H, f'), 1.43 (m, 6H, g+g'), 1.17 (m, 18H, a), 1.05 (m, 6H, h+h'). ^{13}C{^{1}H} NMR (100 MHz, d_4-methanol, δ(ppm)): 162.8 (f), 162.6 (l), 153.8 (p), 138.2 (c), 132.0 (n), 129.3 (d'), 129.3 (m), 129.0 (d), 125.3 (e'), 124.7 (e), 111.9 (o), 64.4 (h), 63.4 (h'), 56.9 (g), 56.3 (g'), 40.5 (q), 35.4 (i'), 34.8 (i), 34.3 (b), 32.0 (a), 28.9 (j'), 28.8 (j), 21.8 (k'), 21.3 (k). IR ($\nu_{c=o}$, cm^{-1}, neat): 1612 (a, terminal), 1377 (s, terminal). MS (MALDI-ToF): m/z 802.4 [LMgZn(OBz^{NMe2})]$^{+}$ (100 %). Calc. for $C_{52}H_{74}O_6N_6MgZn$: C, 64.46; H, 7.70; N, 8.67; Found: 64.60; H, 7.87; N, 8.39 %.

Complex 2f

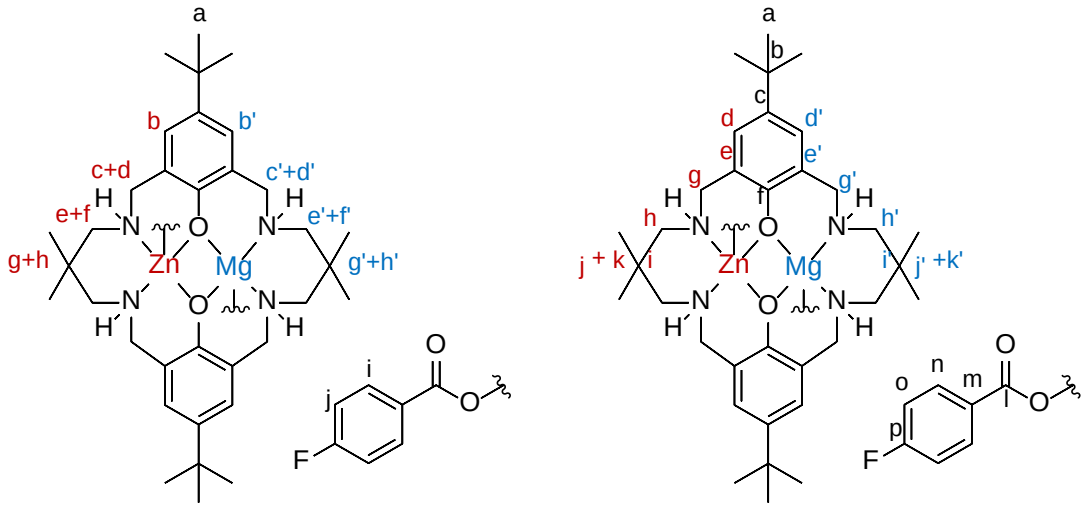

Synthesised on a 1.24 mmol scale. Yielded a white powder (1.05 g, 1.14 mmol, 92 %).

^{1}H NMR (400 MHz, d_4-methanol, δ(ppm)): 7.89 (br s, 4H, i), 6.96 (br s, 4H, j), 6.96 (s, 4H, b+b'), 4.24 (d, $^{2}J_{H-H}$ = 12 Hz, 2H, c), 4.04 (d, $^{2}J_{H-H}$ = 12 Hz, 2H, c'), 3.27 (br m, 4H, d+d'),

2.91 (m, 2H, e), 2.86-2.78 (m, 4H, f+e'), 2.70 (br d, $^{2}J_{H-H}$ = 11 Hz, 2H, f'), 1.42 (m, 6H, g+g'), 1.17 (s, 18H, a), 1.05 (m, 6H, h+h'). $^{13}C\{^{1}H\}$ NMR (100 MHz, d_4-methanol, δ(ppm)): 173.3 (l), 165.7 (d, $^{1}J_{F-C}$ = 248 Hz) (p) 162.8 (f), 138.0 (c), 132.8 (d, $^{3}J_{F-C}$ = 9 Hz) (n), 129.3 (d'), 129.1 (m), 129.0 (d), 125.3 (e'), 124.6 (e), 115.2 (d, $^{2}J_{F-C}$ = 22 Hz) (o), 64.2 (h), 63.4 (h'), 56.9 (g), 56.2 (g'), 35.4 (i'), 34.9 (i), 34.3 (b), 32.0 (a), 28.9 (j'), 28.8 (j), 21.8 (k'), 21.3 (k). $^{19}F\{^{1}H\}$ NMR (377 MHz, d_4-methanol, δ(ppm)): -113.2. IR ($\nu_{c=o}$, cm^{-1}, neat): 1610 (a, terminal), 1570 (a, bridging), 1391 (s, terminal). MS (MALDI-ToF): m/z 777.4 $[LMgZn(OBz^{F})]^{+}$ (100 %). Calc. for $C_{48}H_{62}O_6N_4F_2MgZn$: C, 62.75; H, 6.80; N, 6.10; Found: C, 60.39; H, 7.12; N, 5.88 %.

Complex 2g

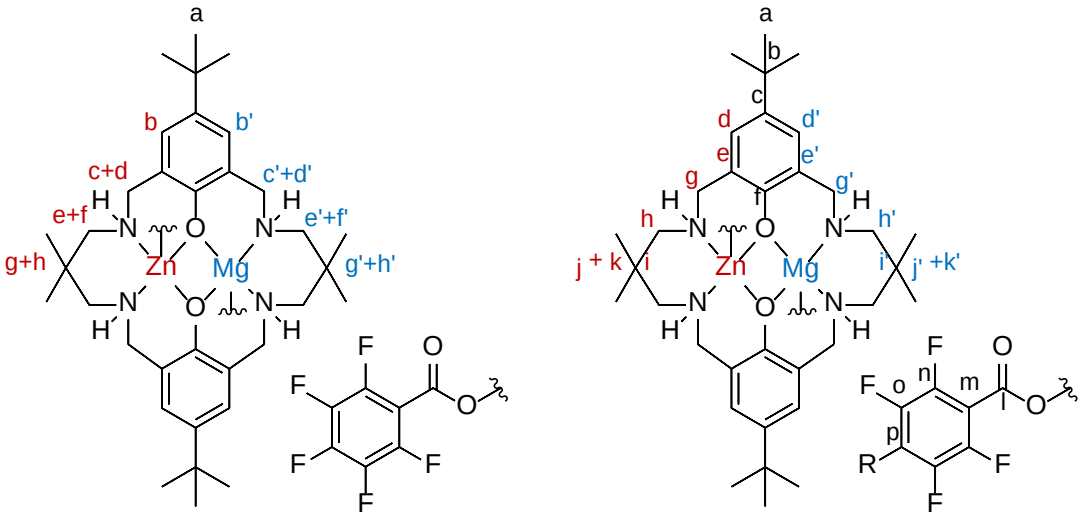

Synthesised on a 0.91 mmol scale. Yielded a white powder (739 mg, 0.70 mmol, 77 %).

^{1}H NMR (400 MHz, d_4-methanol, δ(ppm)): 7.02 (s, 4H, b+b'), 4.25 (m, 2H, c), 4.03 (br m, 2H, c'), 3.27 (br m, 4H d+d'), 2.87 (br m, 2H, e), 2.82-2.73 (m, 4H, f+e'), 2.67 (br m, 2H, f'), 1.23 (m, 18H, a), 1.22 (m, 3H, g), 1.17 (m, 3H, g'), 1.02 (s, 6H, h+h'). $^{13}C\{^{1}H\}$ NMR (100 MHz, d_4-methanol, δ(ppm)): 164.0 (l), 162.5 (f), 138.8 (c), 129.3 (d'), 129.1 (d), 128.1 (m), 125.3 (e'), 124.5 (e), 64.0 (h), 63.2 (h'), 56.8 (g), 56.0 (g'), 35.2 (i'), 34.7 (i), 34.3 (b), 32.0 (a), 28.7 (j'), 28.6 (j), 21.2 (k'), 21.1 (k). The broad resonances, expected for the pentafluorobenzoate co-ligand (n, o, p), appear in the region 138 – 146 ppm but could not be assigned due to significant C–F coupling. $^{19}F\{^{1}H\}$ NMR (377 MHz, d_4-methanol, δ(ppm)): -143.7, -144.6, -157.8, -160.1, -165.4, -165.7. IR ($\nu_{c=o}$, cm^{-1}, neat): 1647 (a, terminal), 1381 (s, terminal). MS (MALDI-ToF): m/z 848 $[LMgZnOBz^{F5}]^{+}$ (50 %). Calc. for $C_{48}H_{54}O_6N_4F_{10}MgZn$: C, 54.25; H, 5.12; N, 5.27; Found: C, 54.13; H, 5.27; N, 5.17 %.

Complex 2h

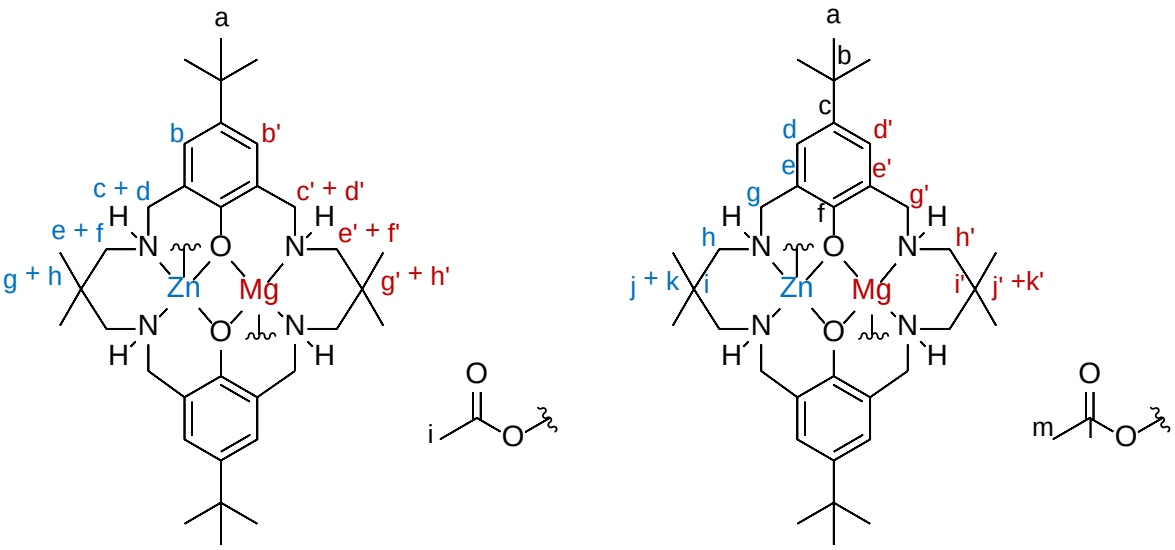

Synthesised on a 0.91 mmol scale. Yielded a white powder (647 mg, 0.85 mmol, 94 %).

^{1}H NMR (400 MHz, d_4-methanol, δ(ppm)): 7.02 (s, 4H, b+b'), 4.22 (m, 2H, c), 3.99 (m, 2H, c'), 3.36-3.21 (m, 4H, d+d'), 2.87-2.79 (m, 2H, e), 2.79-2.68 (m, 4H, f+e'), 2.67-2.62 (m, 2H, f'), 1.70 (br s, 6H, i), 1.26 (m, 18H, a), 1.25-1.23 (m, 6H, g+g'), 1.02-0.98 (m, 6H, h+h'). ^{13}C{^{1}H} NMR (100 MHz, d_4-methanol, δ(ppm)): 179.7 (l), 162.6 (f), 138.3 (c), 129.3 (d'), 129.1 (d), 125.4 (e'), 124.7 (e), 64.2 (h), 63.4 (h'), 56.9 (g), 56.1 (g'), 35.3 (i'), 34.7 (i), 34.4 (b), 32.1 (a), 28.9 (j'), 28.7 (j), 24.0 (m), 21.4 (k'), 21.3 (k). IR ($\nu_{c=o}$, cm^{-1}, neat): 1587 (a, bridging), 1437 (s, bridging). MS (MALDI-ToF): m/z 697.4 $[LMgZnOAc]^+$ (60 %). Calc. for $C_{38}H_{60}O_6N_4MgZn$: C, 60.17; H, 7.97; N, 7.39; Found: C, 60.08; H, 8.03; N, 7.27 %.

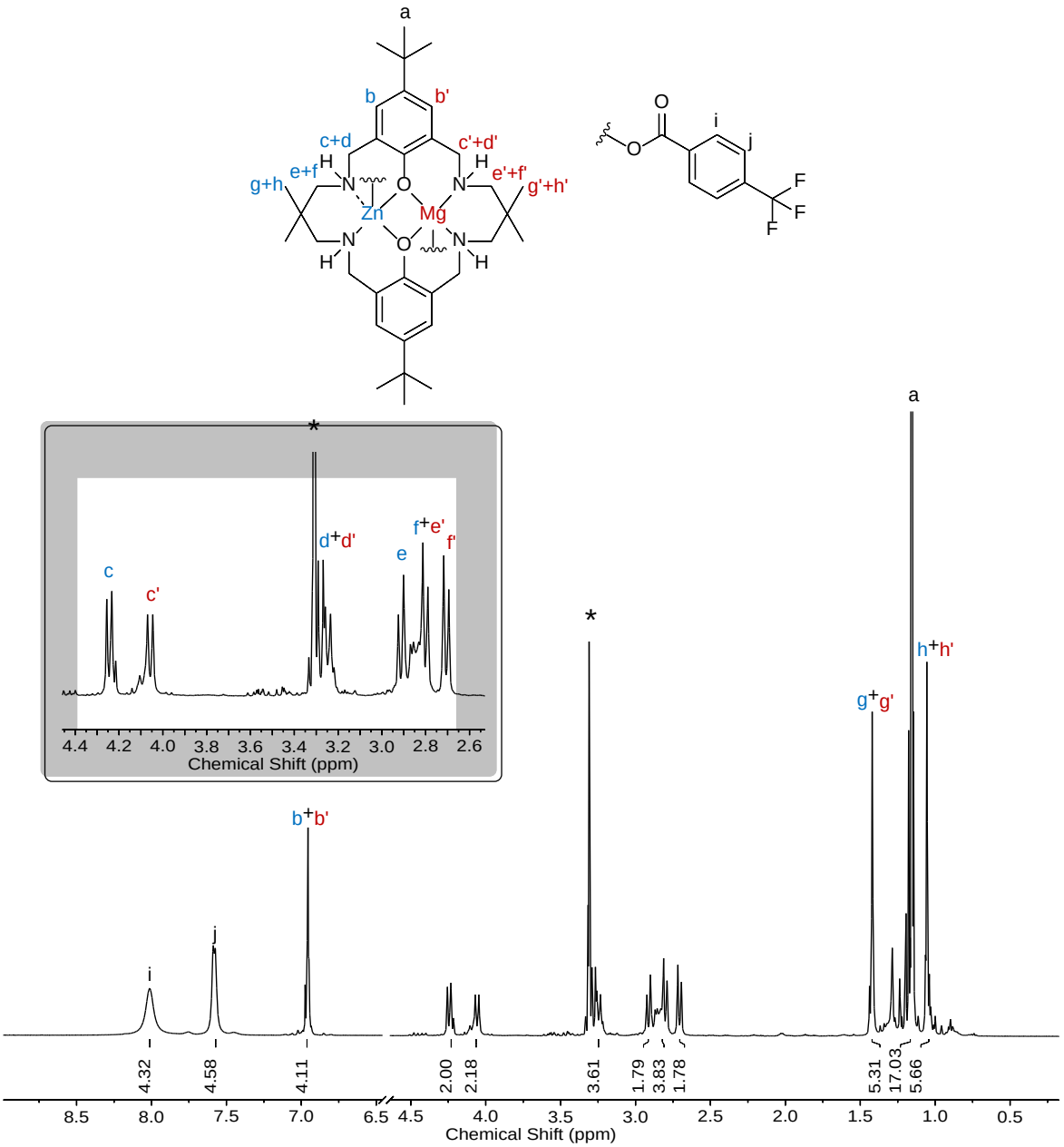

*Figure S1 – ^{1}H NMR spectrum of **2c** in d_4-methanol. Deuterated solvent residue marked with an *.*

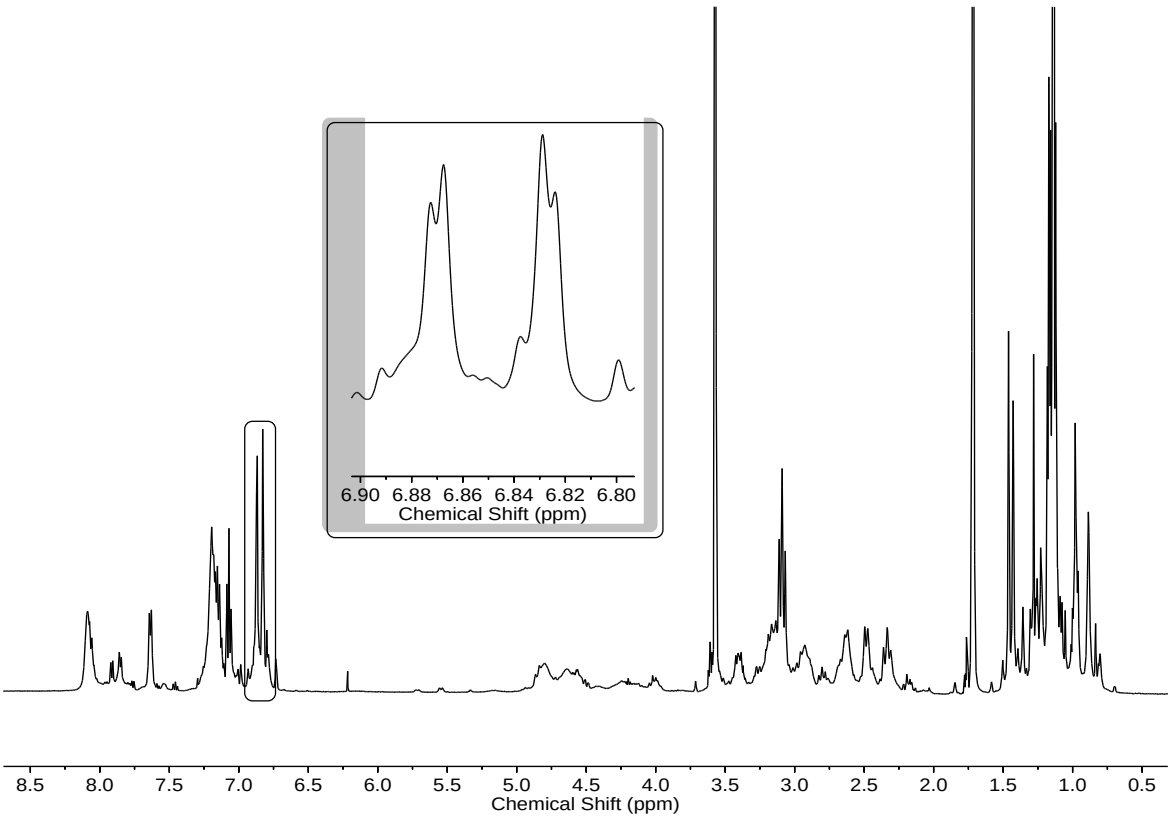

*Figure S2 – ^{1}H NMR spectrum for complex **2a**, in d_8-THF solvent at 298 K, zoomed in on the ligand aromatic region.*

2. **DOSY Spectra**

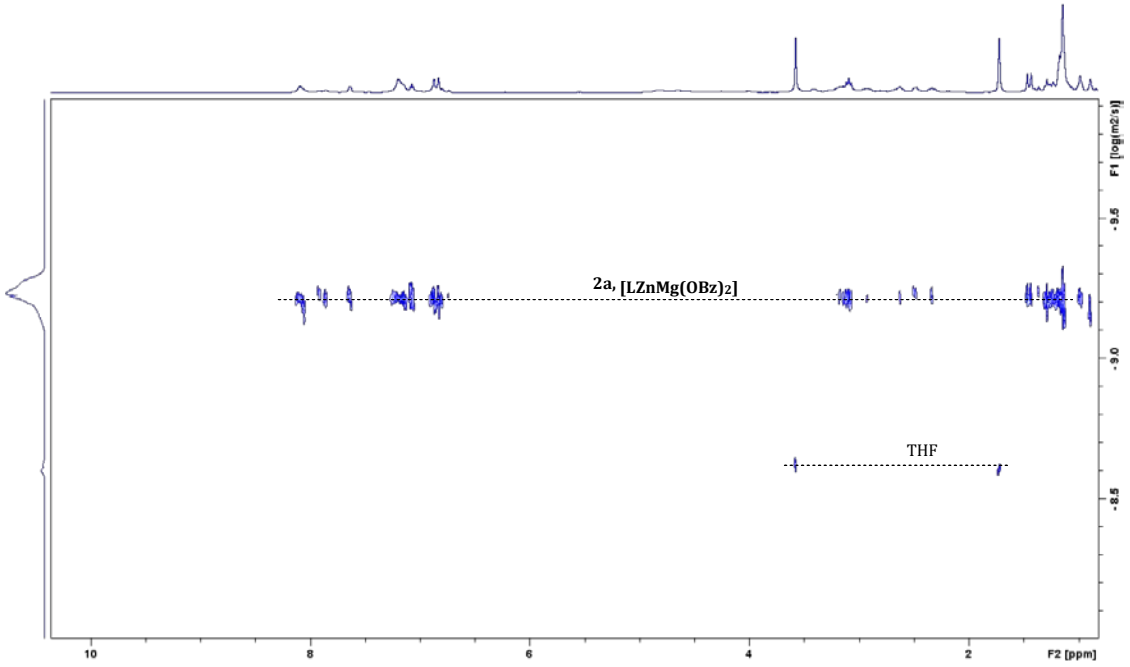

*Figure S3 – DOSY NMR spectrum of complex **2a** in d_8-THF. Through comparison of the diffusion coefficient observed for **2a**, to a calibration plot of known standards in d_8-THF solution,[3] a predicted molecular weight of 1077 g·mol^{-1} was obtained, in relatively close agreement with that of a monomeric species (883 g·mol^{-1}).*

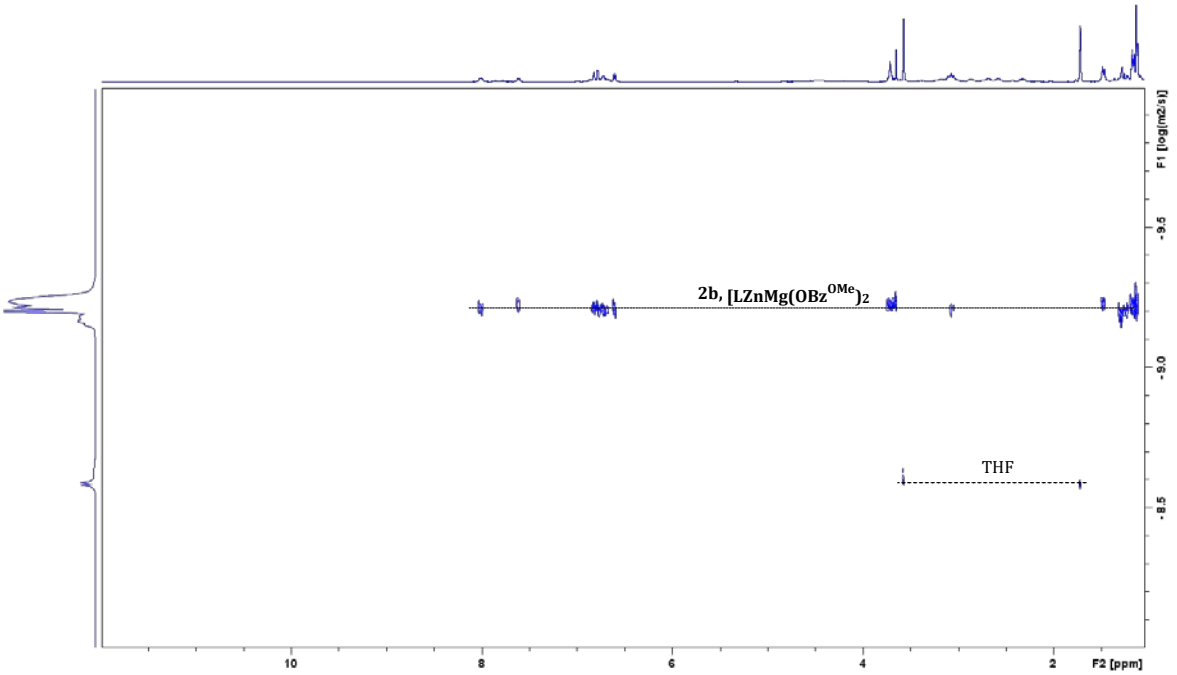

*Figure S4 – DOSY NMR spectrum of complex **2b** in d_8-THF. Through comparison of the diffusion coefficient observed for **2b**, to a calibration plot of known standards in d_8-THF solution,[3] a predicted molecular weight of 1091 g·mol^{-1} was obtained, in relatively close agreement with that of a monomeric species (943 g·mol^{-1}).*

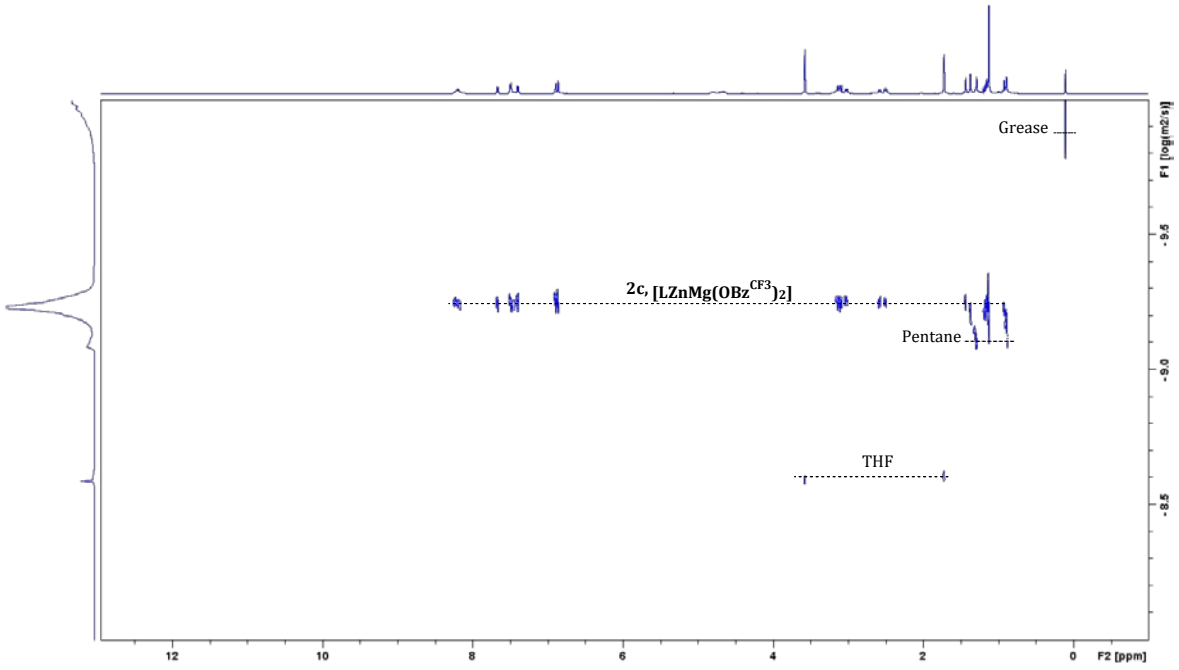

*Figure S5 – DOSY NMR spectrum of complex **2c** in d_8-THF. Through comparison of the diffusion coefficient observed for **2c**, to a calibration plot of known standards in d_8-THF solution,[3] a predicted molecular weight of 1248 g·mol^{-1} was obtained, in relatively close agreement with that of a monomeric species (1098 g·mol^{-1}).*

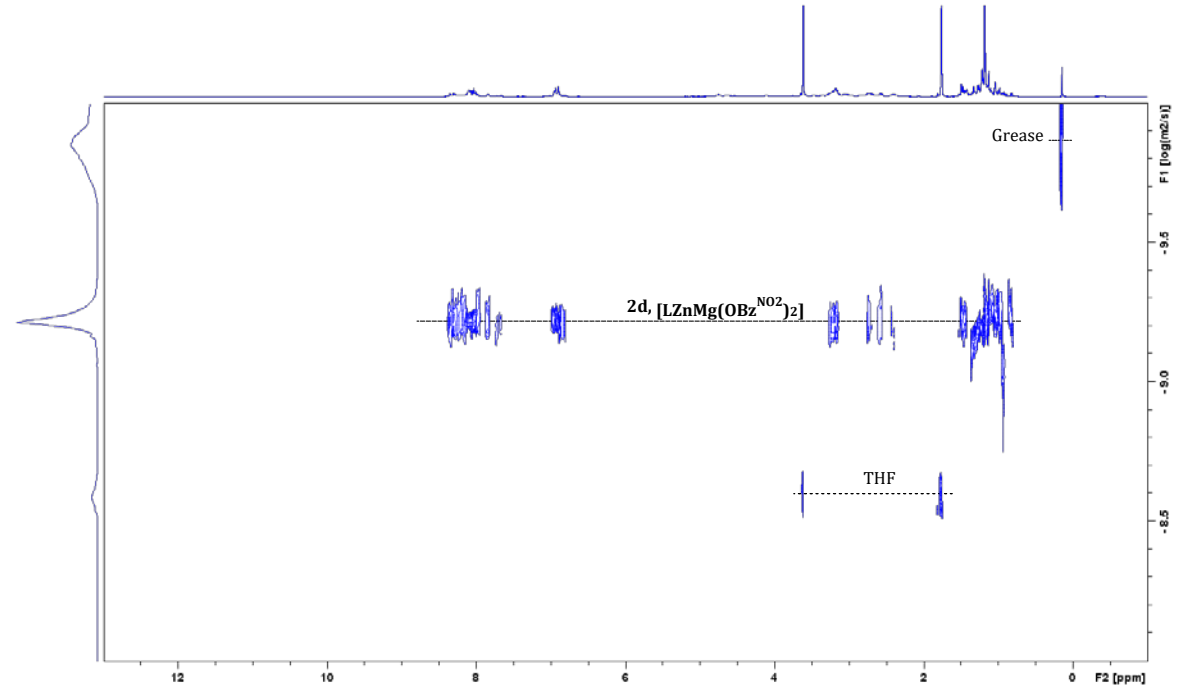

*Figure S6 – DOSY NMR spectrum of complex **2d** in d_8-THF. Through comparison of the diffusion coefficient observed for **2d**, to a calibration plot of known standards in d_8-THF solution,[3] a predicted molecular weight of 1091 g·mol^{-1} was obtained, in close agreement with that of a monomeric species (973 g·mol^{-1}).*

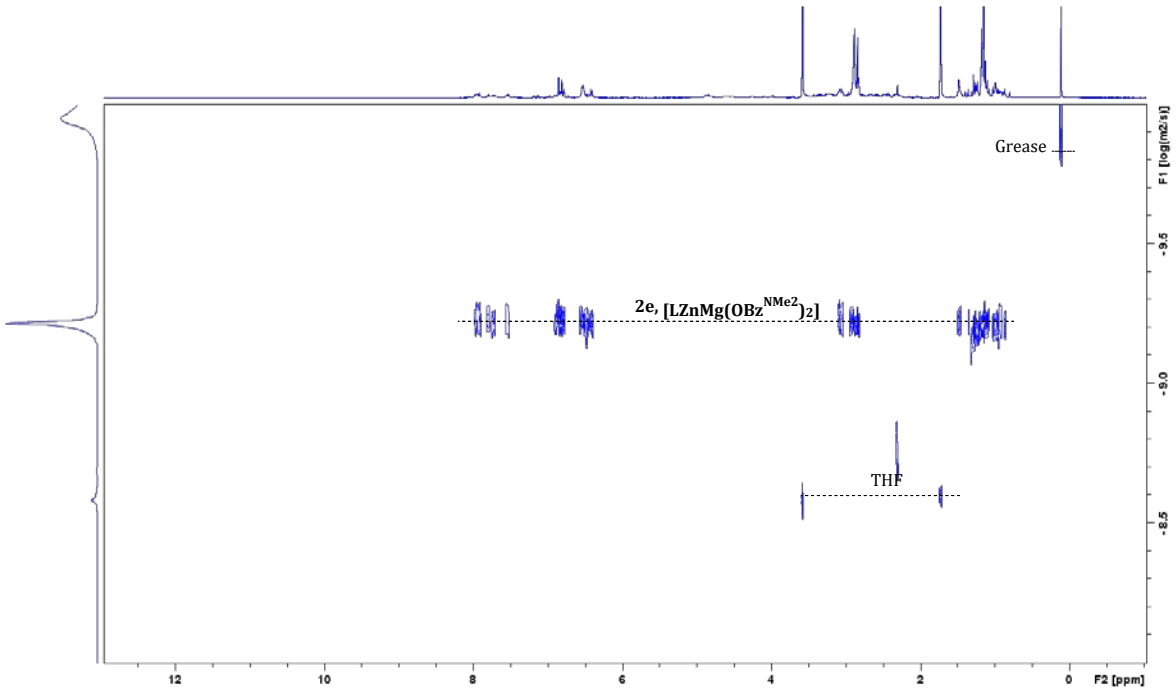

*Figure S7 – DOSY NMR spectrum of complex **2e** in d_8-THF. Through comparison of the diffusion coefficient observed for **2e**, to a calibration plot of known standards in d_8-THF solution,[3] a predicted molecular weight of 1104 g·mol^{-1} was obtained, in close agreement with that of a monomeric species (969 g·mol^{-1}).*

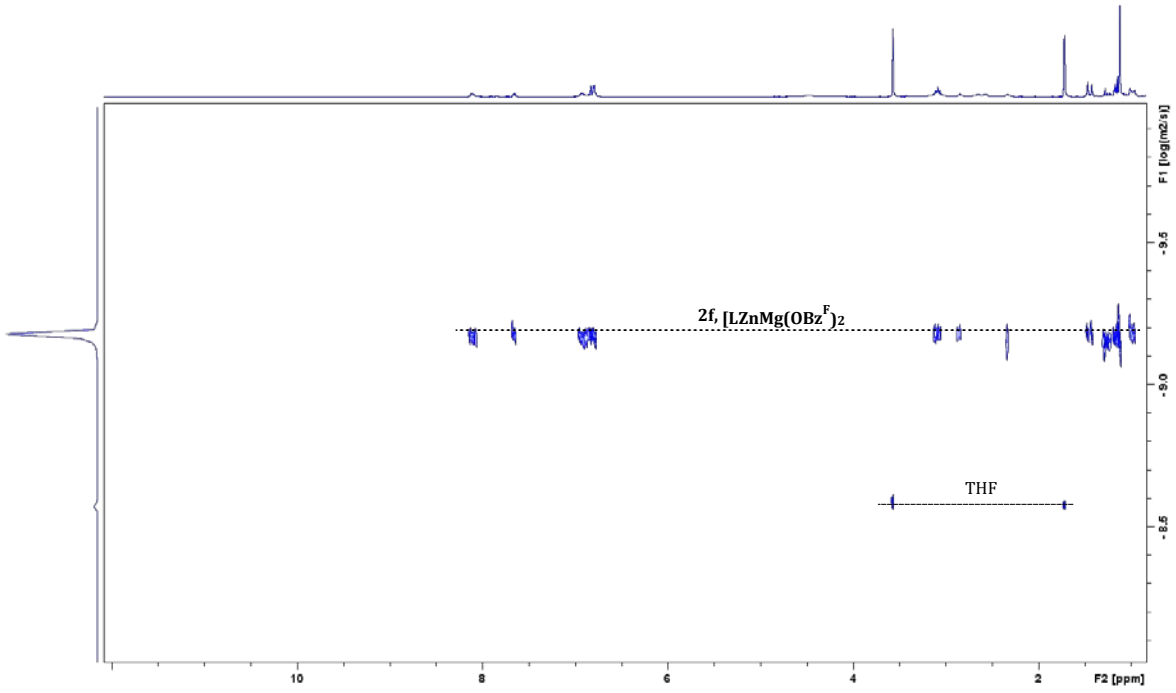

*Figure S8 – DOSY NMR spectrum of complex **2f** in d_8-THF. Through comparison of the diffusion coefficient observed for **2f**, to a calibration plot of known standards in d_8-THF solution,[3] a predicted molecular weight of 938 g·mol^{-1} was obtained, in very close agreement with that of a monomeric species (919 g·mol^{-1}).*

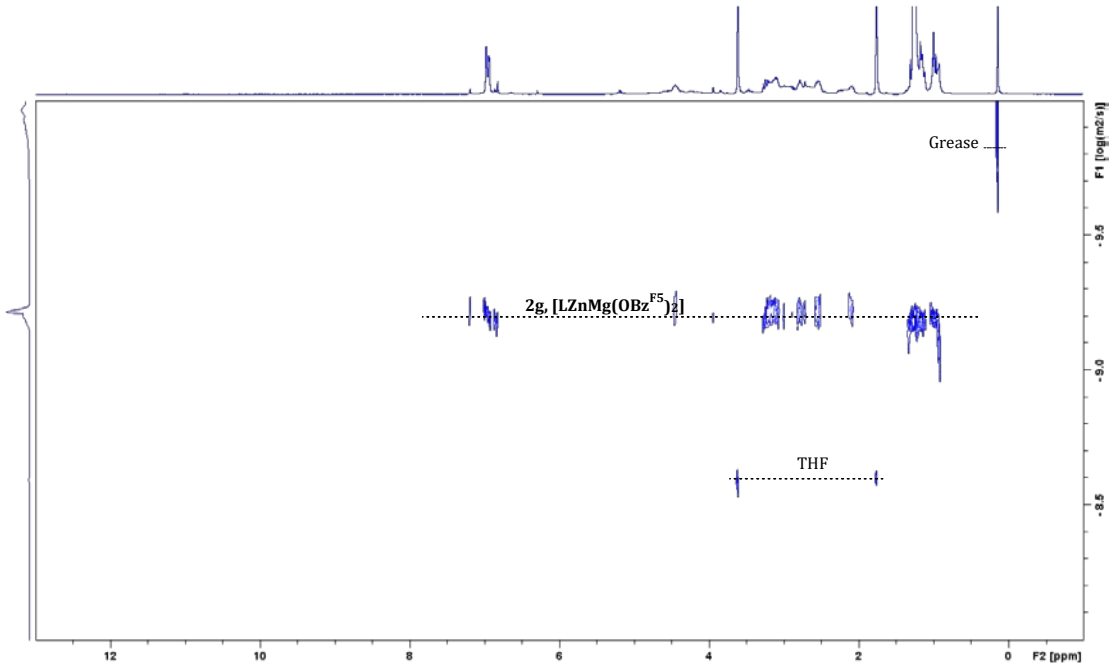

*Figure S9 – DOSY NMR spectrum of complex **2g** in d_8-THF. Through comparison of the diffusion coefficient observed for **2g**, to a calibration plot of known standards in d_8-THF solution,[3] a predicted molecular weight of 1104 g·mol^{-1} was obtained, in very close agreement with that of a monomeric species (1063 g·mol^{-1}).*

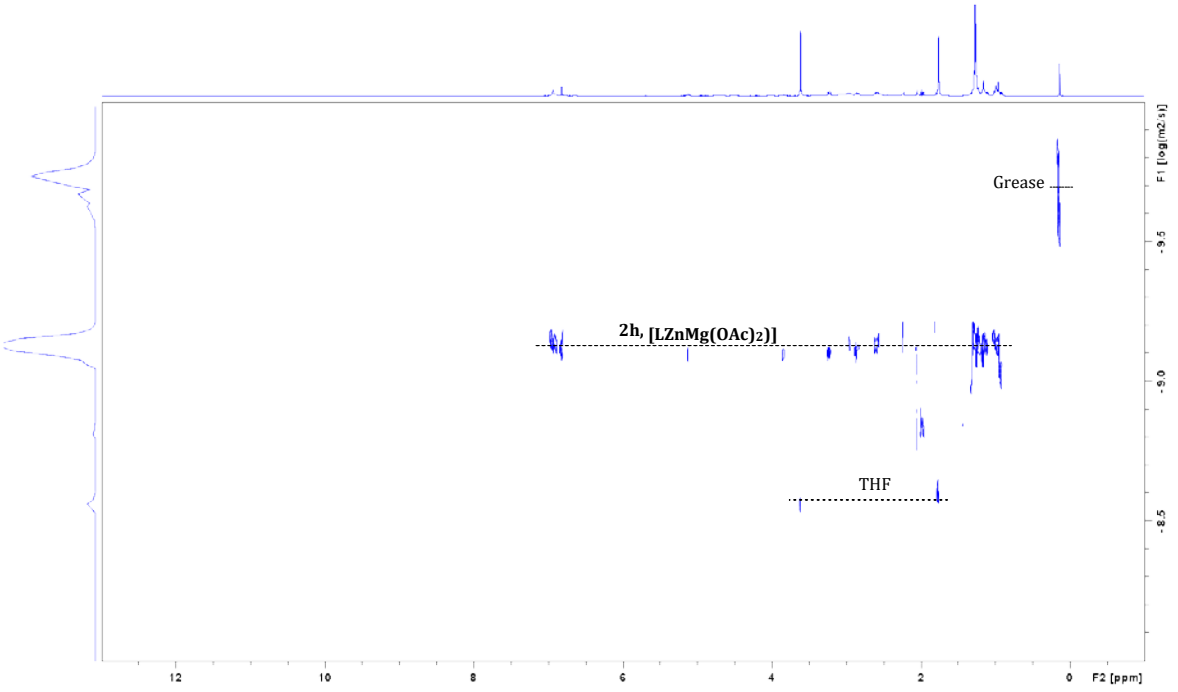

*Figure S10 – DOSY NMR spectrum of complex **2h** in d_8-THF. Through comparison of the diffusion coefficient observed for **2h**, to a calibration plot of known standards in d_8-THF solution,[3] a predicted molecular weight of 777 g·mol^{-1} was obtained, in very close agreement with that of a monomeric species (759 g·mol^{-1}).*

3. **ATR-IR Data (Table 1)**

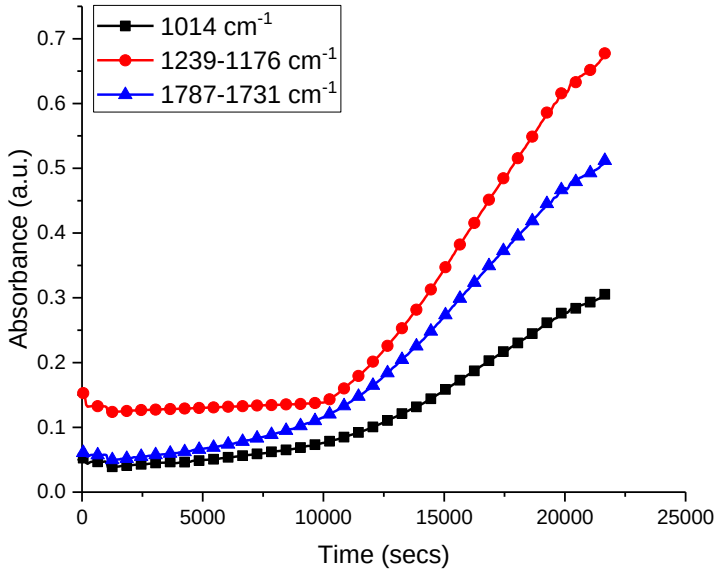

*Figure S11 – ATR-IR spectroscopy plot showing the change in absorbance vs. time for three vibrational modes during the CHO/CO_2 copolymerisation catalysed by **1**. Reaction conditions: 1:1000 catalyst:CHO, 80 °C at 1 bar CO_2 pressure. For clarity, only every 10th data point is shown.*

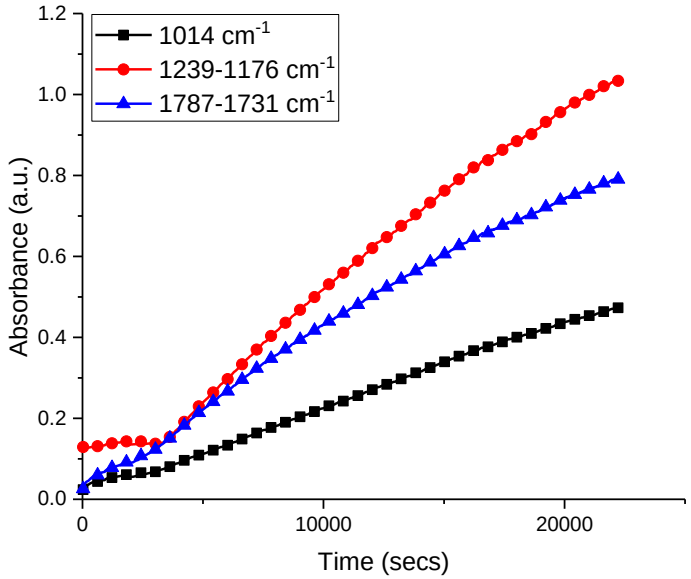

*Figure S12 – ATR-IR spectroscopy plot showing the change in absorbance vs. time for three vibrational modes during the CHO/CO_2 copolymerisation catalysed by **2a**. Reaction conditions: 1:1000 catalyst:CHO, 80 °C at 1 bar CO_2 pressure. For clarity, only every 20th data point is shown.*

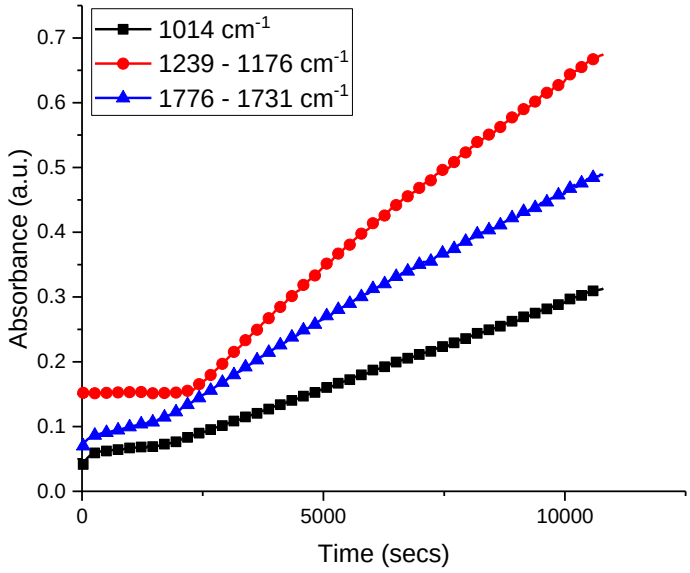

*Figure S13 – ATR-IR spectroscopy plot showing the change in absorbance vs. time for three vibrational modes during the CHO/CO_2 copolymerisation catalysed by **2b**. Reaction conditions: 1:1000 catalyst:CHO, 80 °C at 1 bar CO_2 pressure. For clarity, only every 8th data point is shown.*

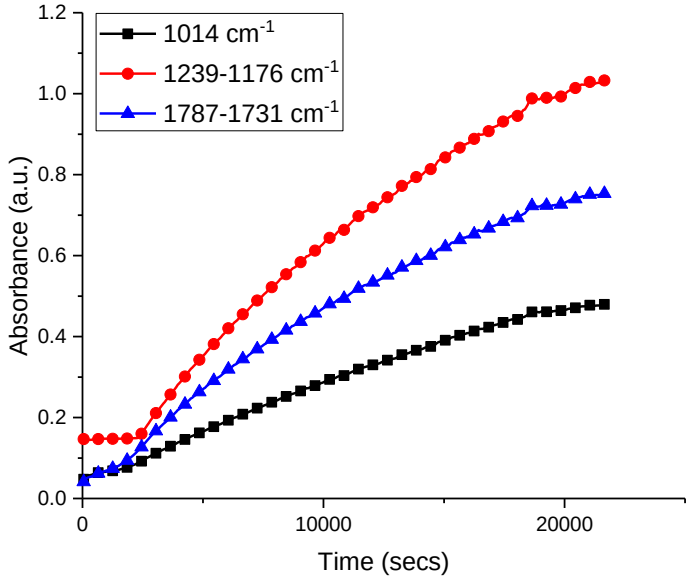

*Figure S14 – ATR-IR spectroscopy plot showing the change in absorbance vs. time for three vibrational modes during the CHO/CO_2 copolymerisation catalysed by **2c**. Reaction conditions: 1:1000 catalyst:CHO, 80 °C at 1 bar CO_2 pressure. For clarity, only every 10th data point is shown.*

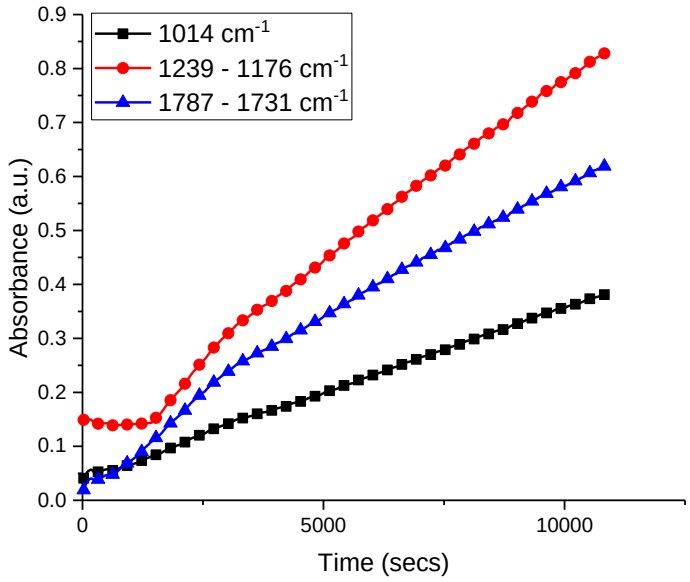

*Figure S15 – ATR-IR spectroscopy plot showing the change in absorbance vs. time for three vibrational modes during the CHO/CO_2 copolymerisation catalysed by **2d**. Reaction conditions: 1:1000 catalyst:CHO, 80 °C at 1 bar CO_2 pressure. For clarity, only every 10th data point is shown.*

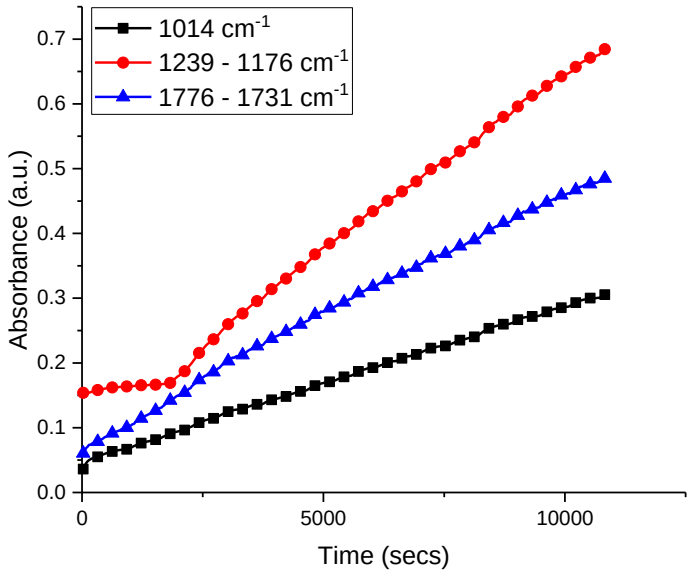

*Figure S16 – ATR-IR spectroscopy plot showing the change in absorbance vs. time for three vibrational modes during the CHO/CO_2 copolymerisation catalysed by **2e**. Reaction conditions: 1:1000 catalyst:CHO, 80 °C at 1 bar CO_2 pressure. For clarity, only every 10th data point is shown*

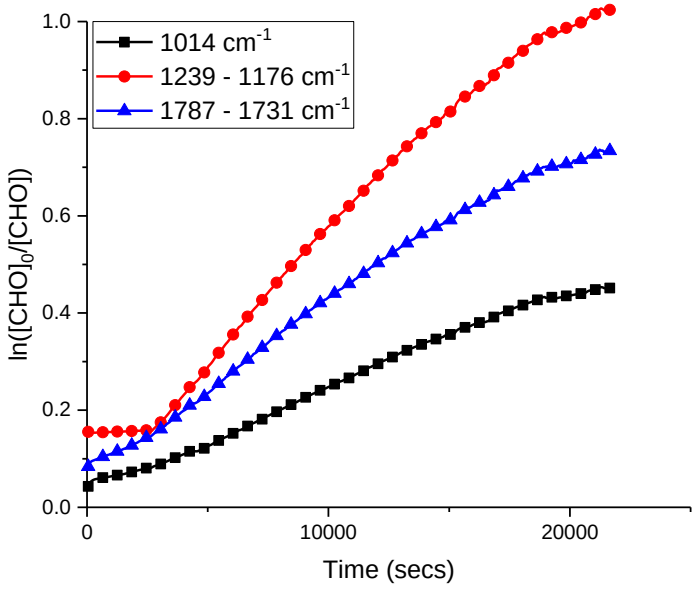

*Figure S17 – ATR-IR spectroscopy plot showing the change in absorbance vs. time for three vibrational modes during the CHO/CO_2 copolymerisation catalysed by **2f**. Reaction conditions: 1:1000 catalyst:CHO, 80 °C at 1 bar CO_2 pressure. For clarity, only every 10th data point is shown.*

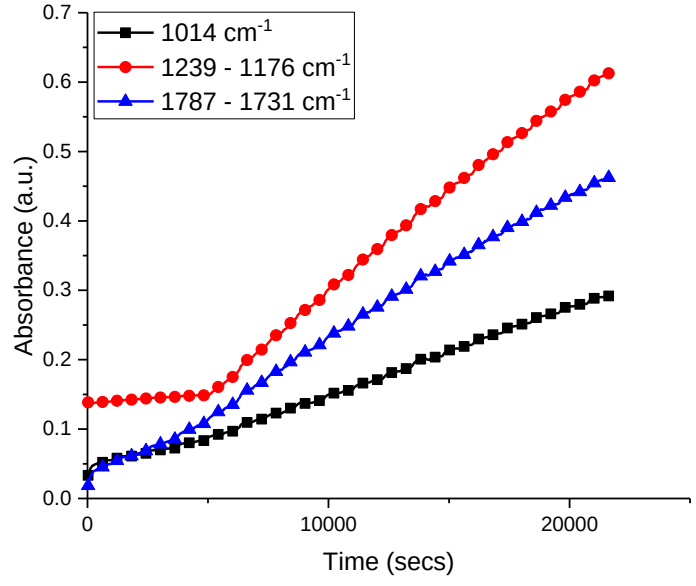

*Figure S18 – ATR-IR spectroscopy plot showing the change in absorbance vs. time for three vibrational modes during the CHO/CO_2 copolymerisation catalysed by **2g**. Reaction conditions: 1:1000 catalyst:CHO, 80 °C at 1 bar CO_2 pressure. For clarity, only every 20th data point is shown.*

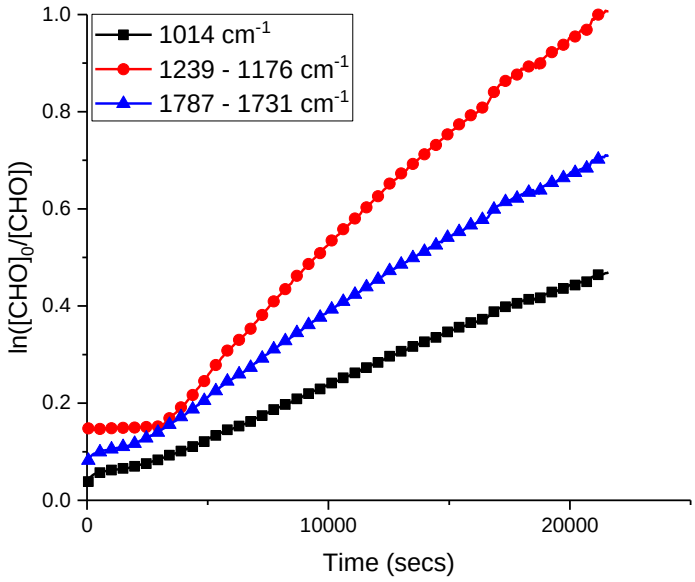

Figure S19 – ATR-IR spectroscopy plot showing the change in absorbance vs. time for three vibrational modes during the CHO/CO_2 copolymerisation catalysed by ***2h****. Reaction conditions: 1:1000 catalyst:CHO, 80 °C at 1 bar CO_2 pressure. For clarity, only every 8th data point is shown.*

4. **Linear Fits to Determine Initial Rate (Table 1)**

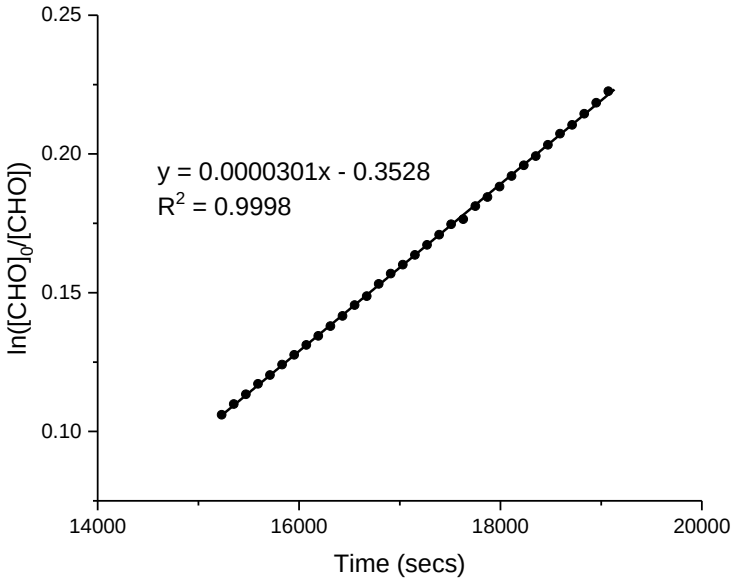

*Figure S20 – Plot of ln([CHO]$_0$/[CHO]) vs. time for CHO/CO_2 copolymerisation catalysed by **1**, for 10-20 % conversion. The gradient of the graph represents k_{obs}, assuming a first order dependence on epoxide. Reaction conditions: 1:1000 catalyst:CHO, 80 °C at 1 bar CO_2 pressure. For clarity, only every 2nd data point is shown.*

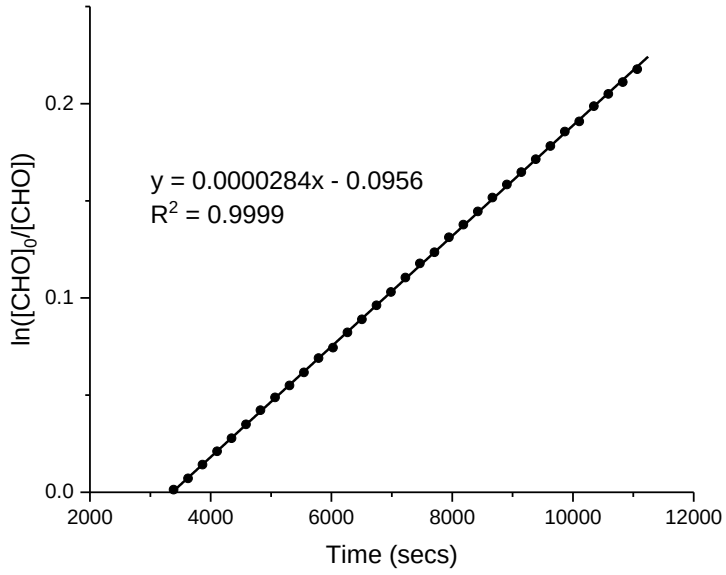

*Figure S21 – Plot of ln([CHO]$_0$/[CHO]) vs. time for CHO/CO_2 copolymerisation catalysed by **2a**. The gradient of the graph represents k_{obs}, assuming a first order dependence on epoxide. Reaction conditions: 1:1000 catalyst:CHO, 80 °C at 1 bar CO_2 pressure. For clarity, only every 9th data point is shown.*

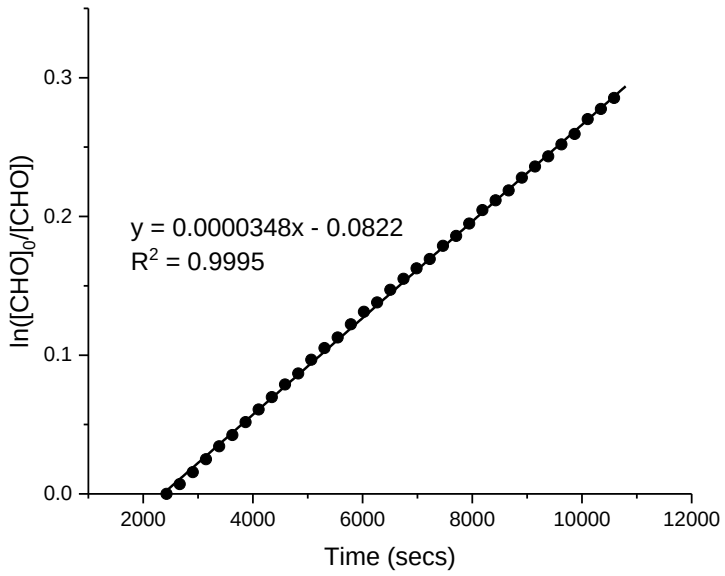

*Figure S22 – Plot of ln([CHO]$_0$/[CHO]) vs. time for CHO/CO_2 copolymerisation catalysed by **2b**. The gradient of the graph represents k_{obs}, assuming a first order dependence on epoxide. Reaction conditions: 1:1000 catalyst:CHO, 80 °C at 1 bar CO_2 pressure. For clarity, only every 8th data point is shown.*

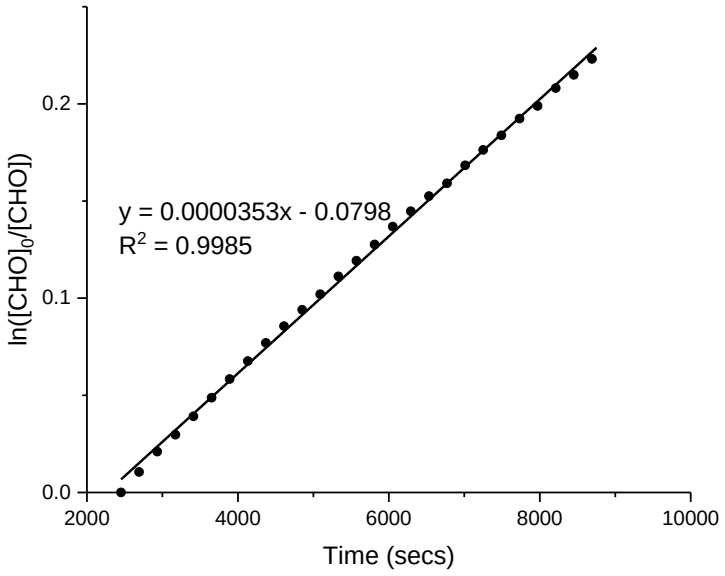

*Figure S23 – Plot of ln([CHO]$_0$/[CHO]) vs. time for CHO/CO_2 copolymerisation catalysed by **2c**. The gradient of the graph represents k_{obs}, assuming a first order dependence on epoxide. Reaction conditions: 1:1000 catalyst:CHO, 80 °C at 1 bar CO_2 pressure. For clarity, only every 4th data point is shown.*

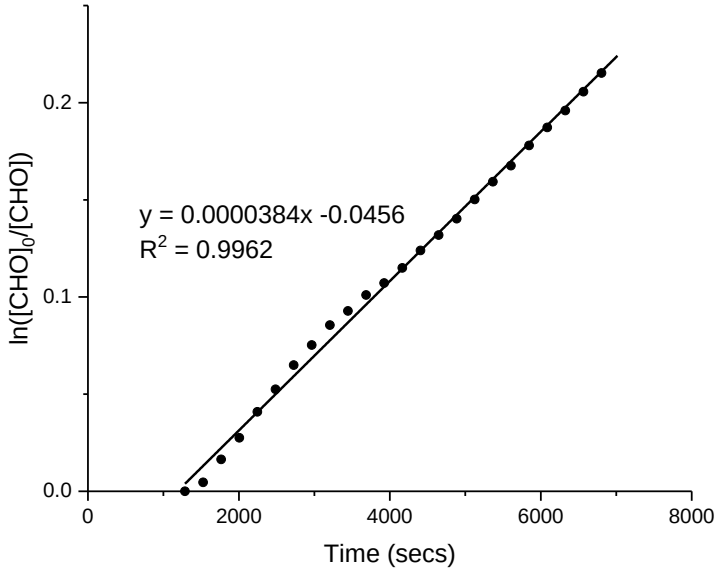

*Figure S24 – Plot of ln([CHO]$_0$/[CHO]) vs. time for CHO/CO_2 copolymerisation catalysed by **2d**. The gradient of the graph represents k_{obs}, assuming a first order dependence on epoxide. Reaction conditions: 1:1000 catalyst:CHO, 80 °C at 1 bar CO_2 pressure. For clarity, only every 8th data point is shown.*

.

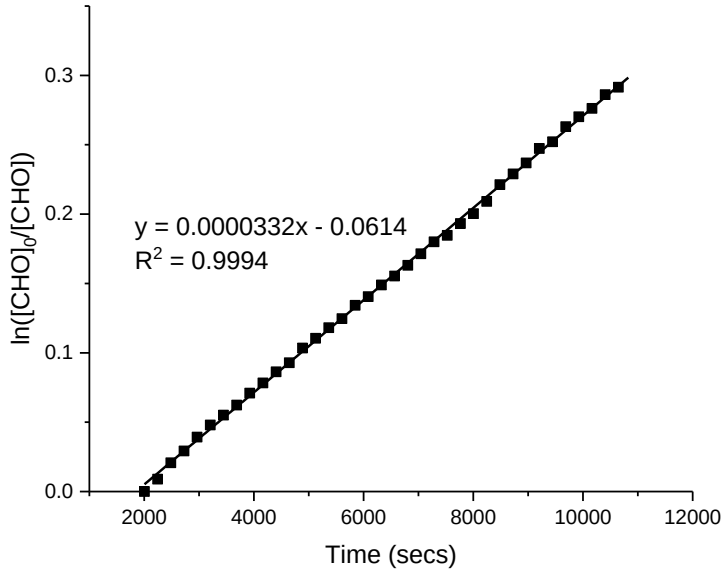

*Figure S25 – Plot of ln([CHO]$_0$/[CHO]) vs. time for CHO/CO_2 copolymerisation catalysed by **2e**. The gradient of the graph represents k_{obs}, assuming a first order dependence on epoxide. Reaction conditions: 1:1000 catalyst:CHO, 80 °C at 1 bar CO_2 pressure. For clarity, only every 8th data point is shown.*

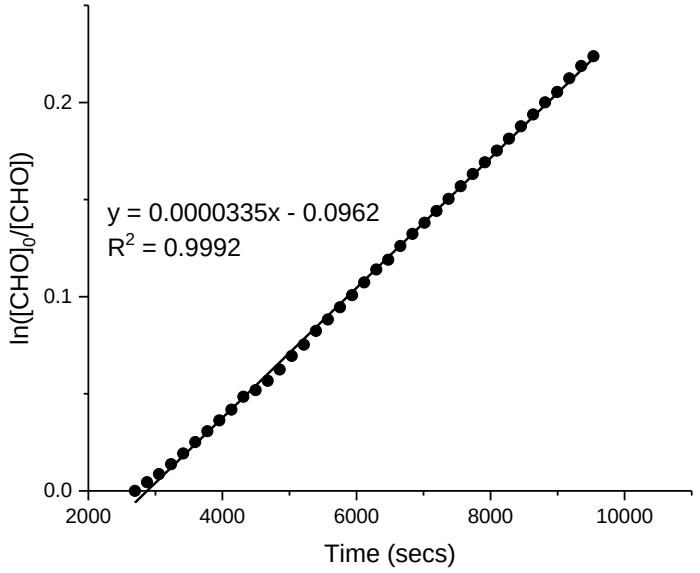

Figure S26 – Plot of ln([CHO]$_0$/[CHO]) vs. time for CHO/CO_2 copolymerisation catalysed by ***2f****. The gradient of the graph represents k_{obs}, assuming a first order dependence on epoxide. Reaction conditions: 1:1000 catalyst:CHO, 80 °C at 1 bar CO_2 pressure. For clarity, only every 3rd data point is shown.*

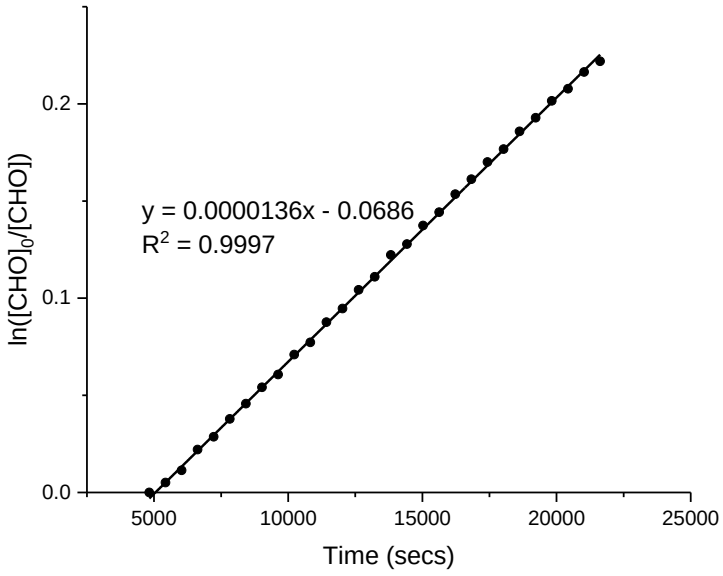

Figure S27 – Plot of ln([CHO]$_0$/[CHO]) vs. time for CHO/CO_2 copolymerisation catalysed by ***2g****. The gradient of the graph represents k_{obs}, assuming a first order dependence on epoxide. Reaction conditions: 1:1000 catalyst:CHO, 80 °C at 1 bar CO_2 pressure. For clarity, only every 20th data point is shown.*

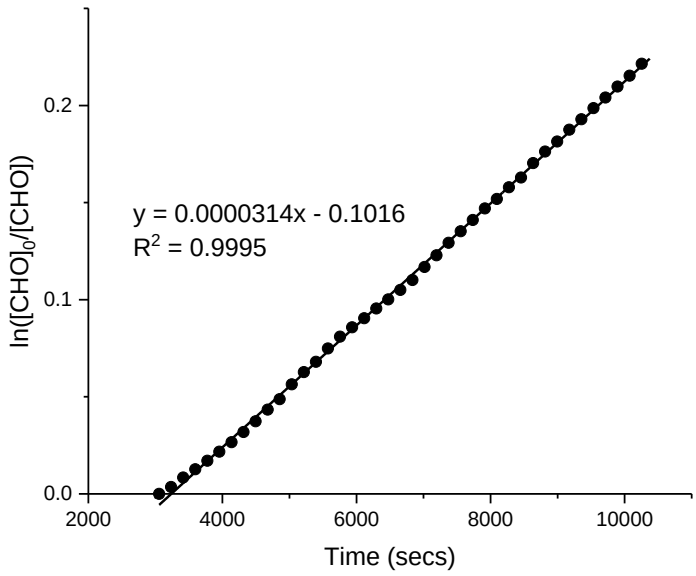

Figure S28 – Plot of ln([CHO]$_0$/[CHO]) vs. time for CHO/CO_2 copolymerisation catalysed by ***2h****. The gradient of the graph represents k_{obs}, assuming a first order dependence on epoxide. Reaction conditions: 1:1000 catalyst:CHO, 80 °C at 1 bar CO_2 pressure. For clarity, only every 3rd data point is shown.*

5. **Characterisation of Poly(cyclohexene carbonate) (Table 1)**

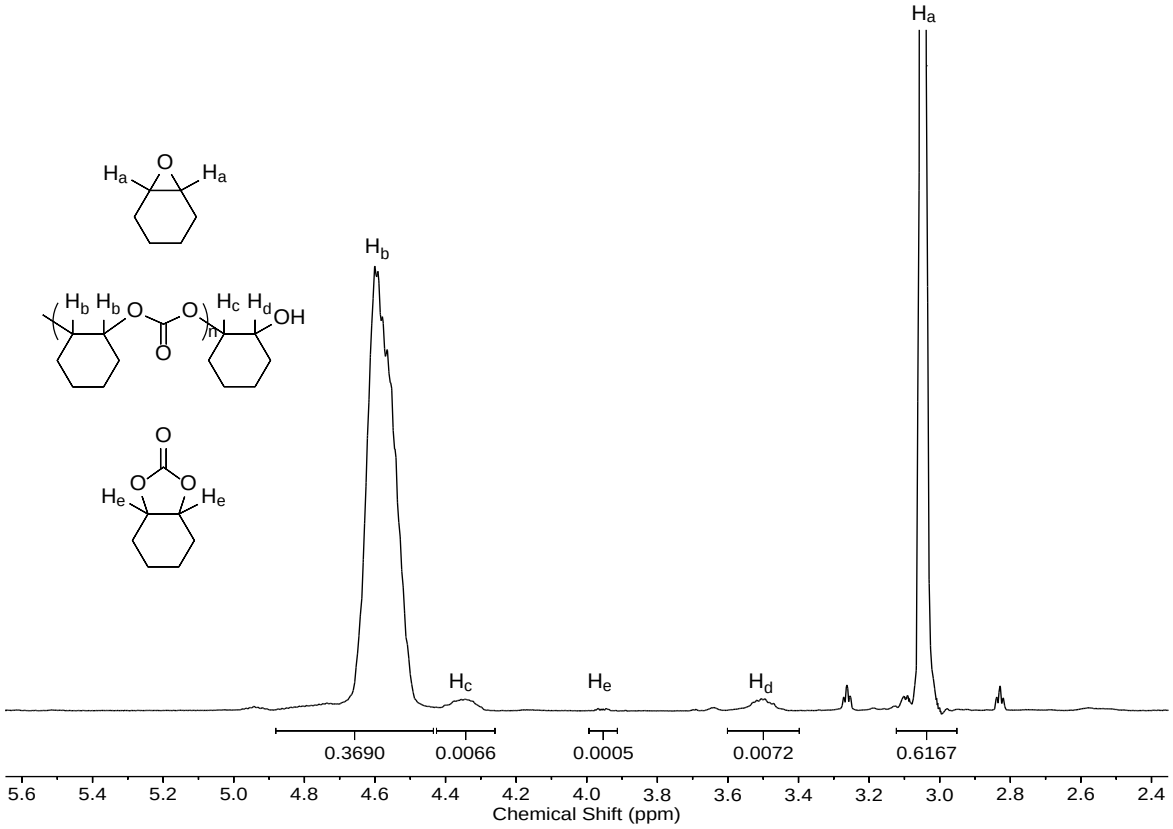

Figure S29 – Representative ^{1}H NMR spectrum of the crude product from the copolymerisation of CO_2 with CHO; the spectra are used to calculate selectivity and TON, in $CDCl_3$. Polyether resonances were not observed.

SEC Data (Table 1)

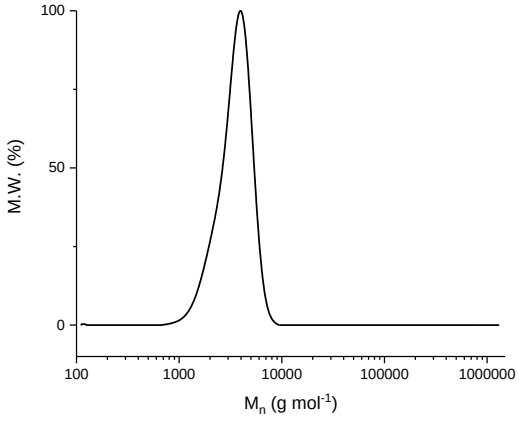

*Figure S30 – SEC plot of M_n for catalyst **1** at 80 °C under 1 bar CO_2 for 6 hours.*

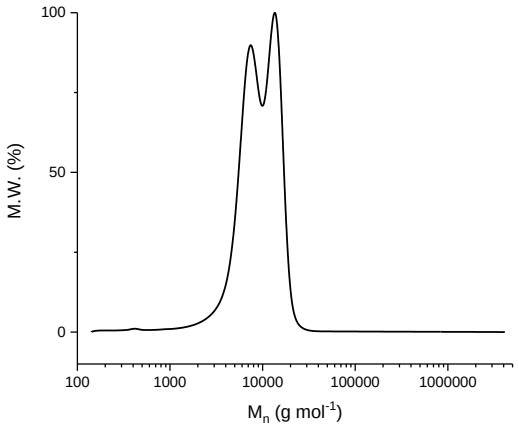

*Figure S31 – SEC plot of M_n for catalyst **2a** at 80 °C under 1 bar CO_2 for 6 hours.*

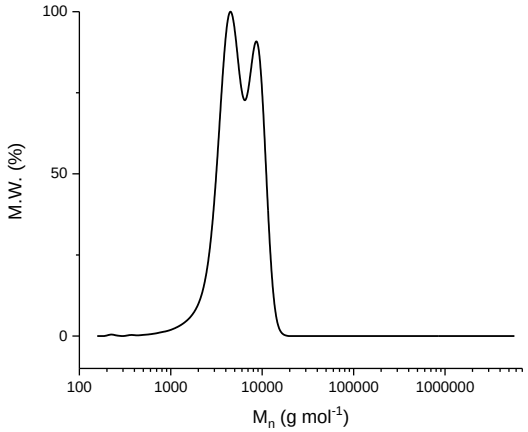

*Figure S32 – SEC plot of M_n for catalyst **2b** at 80 °C under 1 bar CO_2 for 3 hours.*

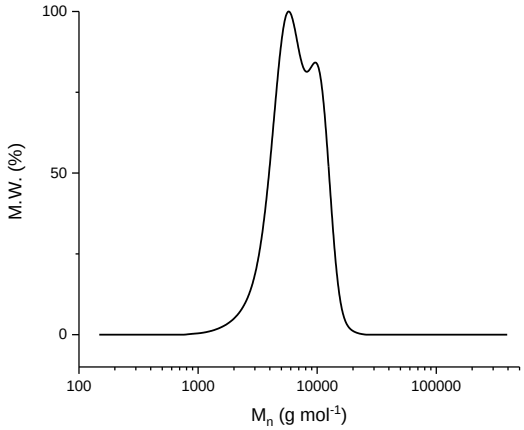

*Figure S33 – SEC plot of M_n for catalyst **2c** at 80 °C under 1 bar CO_2 for 6 hours.*

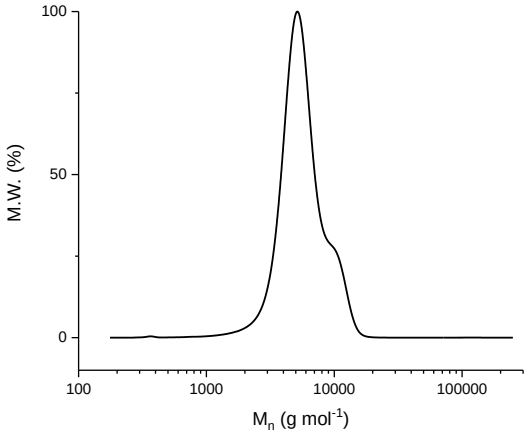

*Figure S34 – SEC plot of M_n for catalyst **2d** at 80 °C under 1 bar CO_2 for 3 hours.*

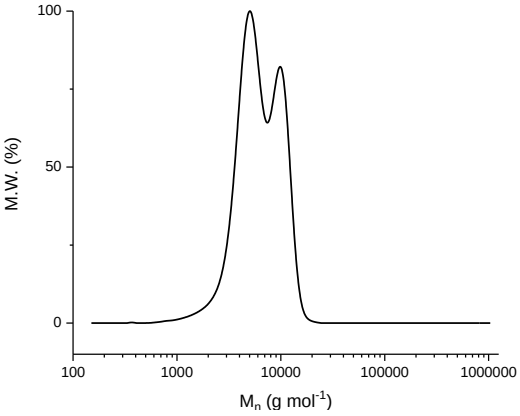

*Figure S35 – SEC plot of M_n for catalyst **2e** at 80 °C under 1 bar CO_2 for 3 hours.*

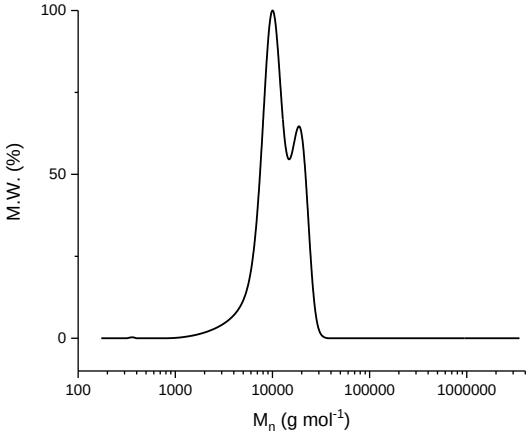

*Figure S36 – SEC plot of M_n for catalyst **2f** at 80 °C under 1 bar CO_2 for 6 hours.*

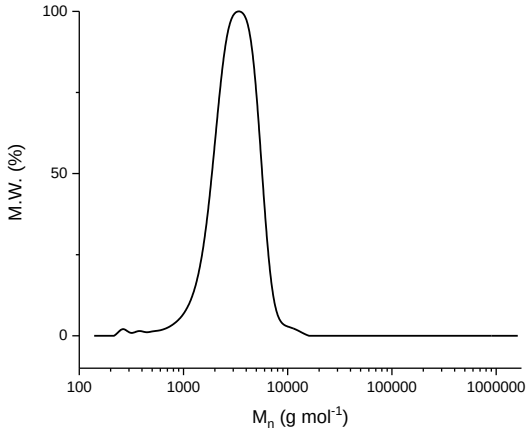

*Figure S37 – SEC plot of M_n for catalyst **2g** at 80 °C under 1 bar CO_2 for 6 hours.*

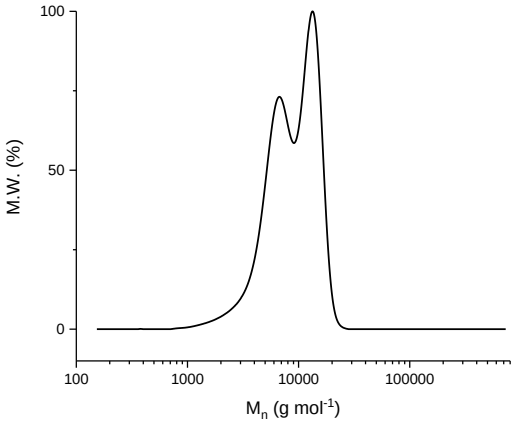

*Figure S38 – SEC plot of M_n for catalyst **2h** at 80 °C under 1 bar CO_2 for 6 hours.*

6. Epoxide/CO_2 Copolymerisation Data

Table S1 – CPO/CO_2 ROCOP Data using Catalyst 2b.[a]

Pressure (bar)	Catalyst (mol%)	Time (h)	CO_2 (%)[b]	Polymer (%)[c]	TON[d]	TOF (h^{-1})[e]	M_n [Đ][f]
1	0.1	6	> 99	> 99	179	30	10200 [1.04] 4500 [1.13]
1	0.1	24	> 99	> 99	520	22	17600 [1.05] 5600 [1.36]
20	0.01	24	> 99	> 99	1825	76	41800 [1.03] 15100 [1.25]

a) Reactions were conducted at 80 °C. b) Determined by ^{1}H NMR spectroscopy ($CDCl_3$) by integrating the normalised resonances for polycarbonate (4.94 ppm) and cyclic carbonate signals (Fig. S39). c) Determined by ^{1}H NMR spectroscopy ($CDCl_3$) by integrating the normalised resonances for carbonate (4.94 ppm) and ether signals (Fig. S39). d) TON = number of moles of cyclopentene oxide consumed/number of moles of catalyst. e) TOF = number of moles of CPO consumed per mole of catalyst per hour. f) Determined by SEC in THF against polystyrene standards and the dispersity is given in brackets (Fig. S40-42).

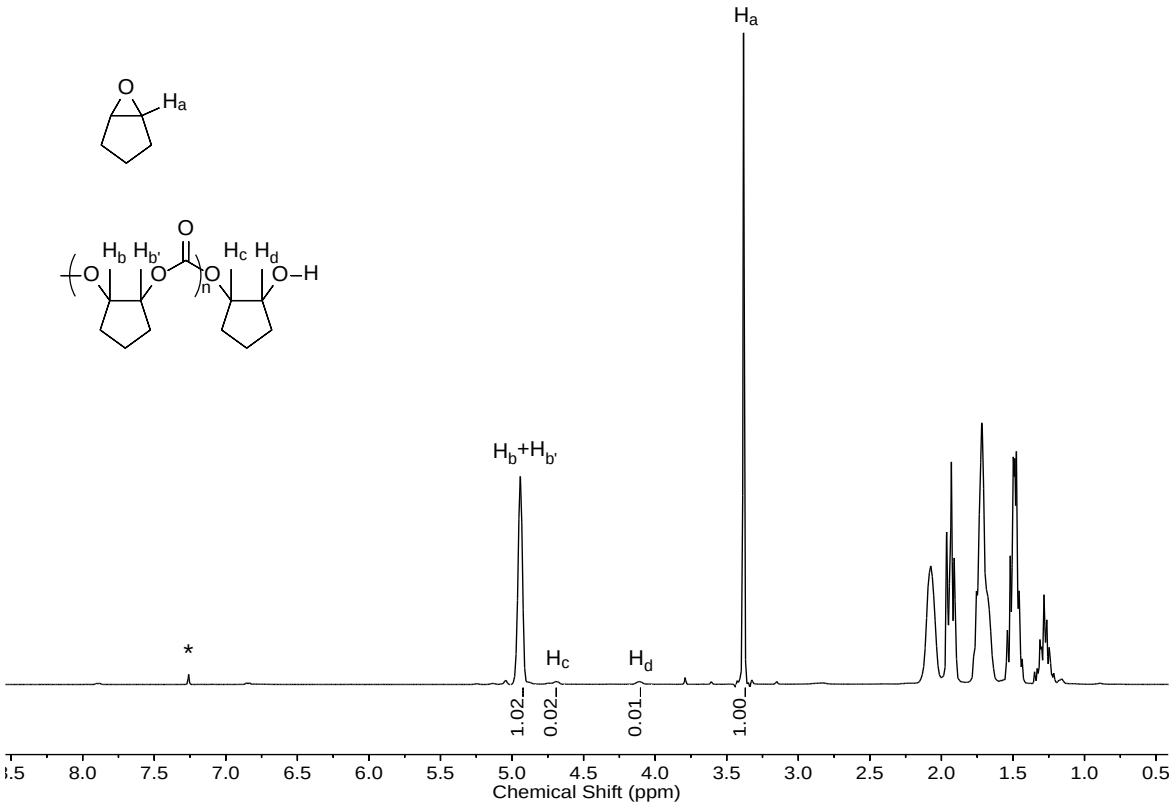

*Figure S39 – ^{1}H NMR spectrum of the crude reaction mixture for the copolymerisation of CPO and CO_2 in $CDCl_3$ at 298 K, used to calculate the TON and selectivity for the copolymerisation. Polyether resonances were not observed. $CDCl_3$ residual solvent signal marked with *.*

SEC Data (Table S1)

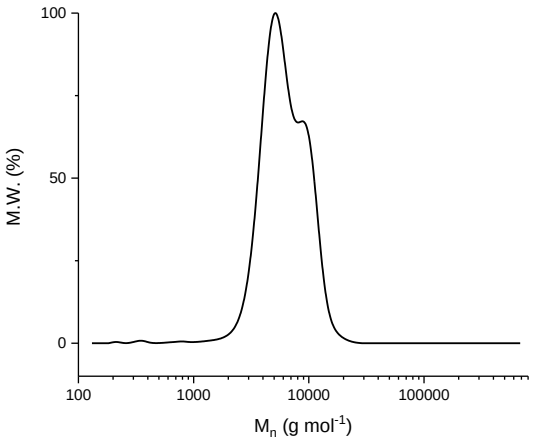

*Figure S40 – SEC plot of M_n for catalyst **2b** with CPO at 80 °C under 1 bar CO_2 for 6 hours at 0.1 mol% catalyst loading.*

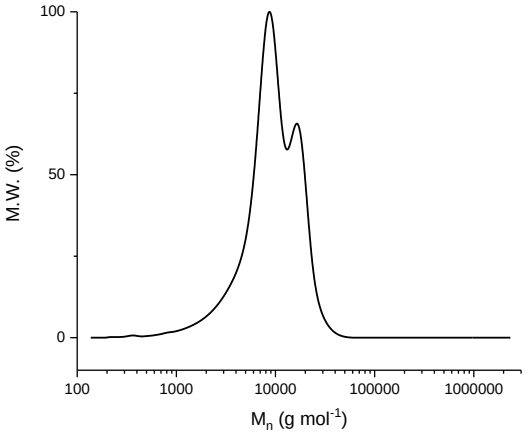

*Figure S41 – SEC plot of M_n for catalyst **2b** with CPO at 80 °C under 1 bar CO_2 for 24 hours at 0.1 mol% catalyst loading.*

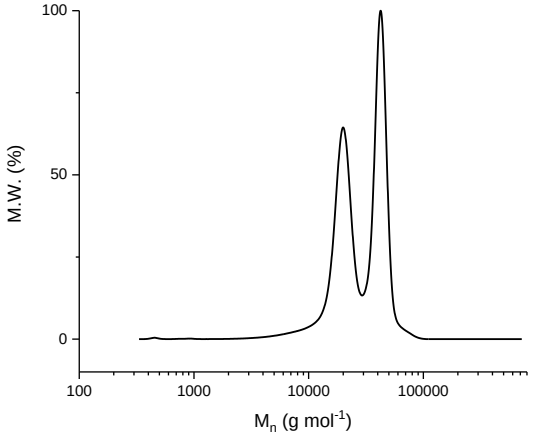

*Figure S42 – SEC plot of M_n for catalyst **2b** with CPO at 80 °C under 20 bar CO_2 for 24 hours at 0.01 mol% catalyst loading.*

Table S2 – Epoxide/CO_2 ROCOP Data for Catalyst 2b with a range of epoxides.[a]

Epoxide	ρCO_2 (bar)	**2b** (mol%)	Time (h)	CO_2[b] (%)	Polymer[c] (%)	TON[d]	M_n [$Đ$][e]
4-Vinyl-1-cyclohexene 1,2-epoxide (v-CHO)	1	0.1	6	> 99	> 99	428	31000 [1.04] 12200 [1.19]
1,4-Cyclohexandiene oxide (CHDO)	1	0.1	6	> 99	74	6	2400 [1.27]
1,2-Propene oxide (PO)	20	0.01	72	98	26	593	4000 [1.20] 1200 [1.20]
3,4-Epoxytetrahydrofuran (ETHF)	1	0.1	6	> 99	93	83	1100 [1.64]
3,4-Epoxytetrahydrofuran (ETHF)	1	0.1	24	> 99	98	289	1300 [1.76]

a) All reactions were conducted at 80 °C. Reactions at 1 bar pressure of CO_2 were carried out in a Schlenk tube with magnetic stirring. Reactions at 20 bar were carried out in a Parr high pressure vessel with an impeller. b) Determined by ^{1}H NMR spectroscopy ($CDCl_3$) by integrating the normalised resonances for polycarbonate and cyclic carbonate signals. c) Determined by ^{1}H NMR spectroscopy ($CDCl_3$) by integrating the normalised resonances for carbonate and ether signals. d) TON = number of moles of epoxide consumed/number of moles of catalyst. e) Determined by SEC in THF against polystyrene standards. The dispersity is given in brackets.

7. Polymerisation Kinetic Data

To investigate the polymerisation kinetics of catalyst **2e**, copolymerisation runs were conducted at $[CHO]_0$ = 5 M in diethyl carbonate and were monitored until high epoxide conversions (>80 %). The data were fit to an exponential and the observed rate constant was extracted. The raw data was fit in OriginPro 2017 as an exponential and then iteratively fit until it converged. Other non-linear models were tested, but resulted in much poorer fits as evidenced by lower R^2 coefficients.

Raw Data for Figure 1a

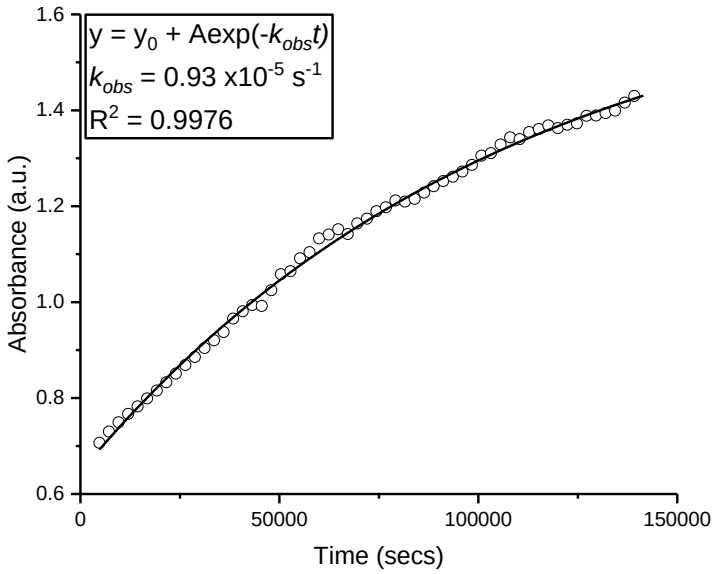

*Figure S43 – ATR-IR spectroscopy plot showing the change in absorbance vs. time plot for the 1239-1176 cm^{-1} vibrational band, during the CHO/CO_2 copolymerisation catalysed by **2e**. Reaction conditions: $[CHO]_0$ = 5 M in diethyl carbonate, $[\mathbf{2e}]_0$ = 2.5 mM, 80 °C at 1 bar CO_2 pressure. For clarity, only every 40th data point is shown.*

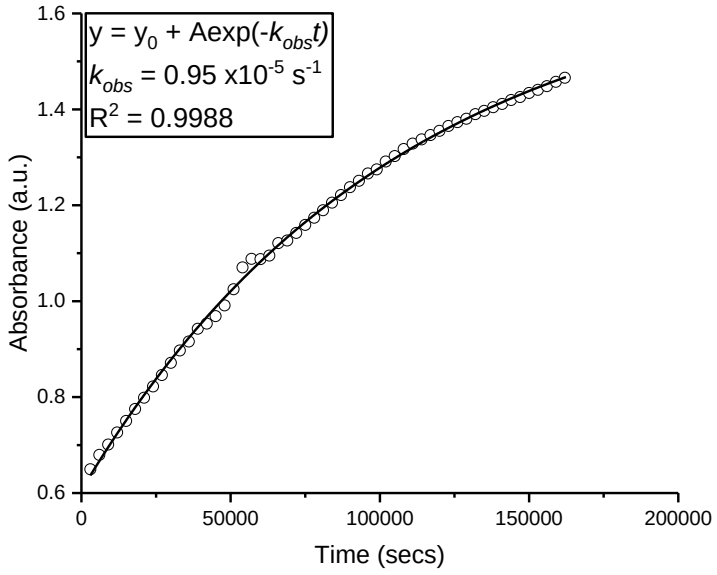

*Figure S44 – ATR-IR spectroscopy plot showing the change in absorbance vs. time plot for the 1239-1176 cm^{-1} vibrational band, during the CHO/CO_2 copolymerisation catalysed by **2e**. Reaction conditions: $[CHO]_0$ = 5 M in diethyl carbonate, $[\mathbf{2e}]_0$ = 3.1 mM, 80 °C at 1 bar CO_2 pressure. For clarity, only every 40th data point is shown.*

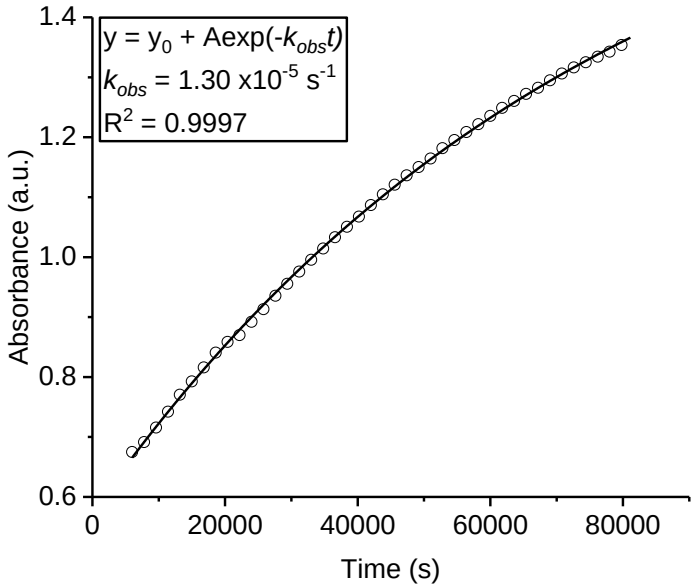

*Figure S45 – ATR-IR spectroscopy plot showing the change in absorbance vs. time plot for the 1239-1176 cm^{-1} vibrational band, during the CHO/CO_2 copolymerisation catalysed by **2e**. Reaction conditions: $[CHO]_0$ = 5 M in diethyl carbonate, $[\mathbf{2e}]_0$ = 3.75 mM, 80 °C at 1 bar CO_2 pressure. For clarity, only every 40th data point is shown.*

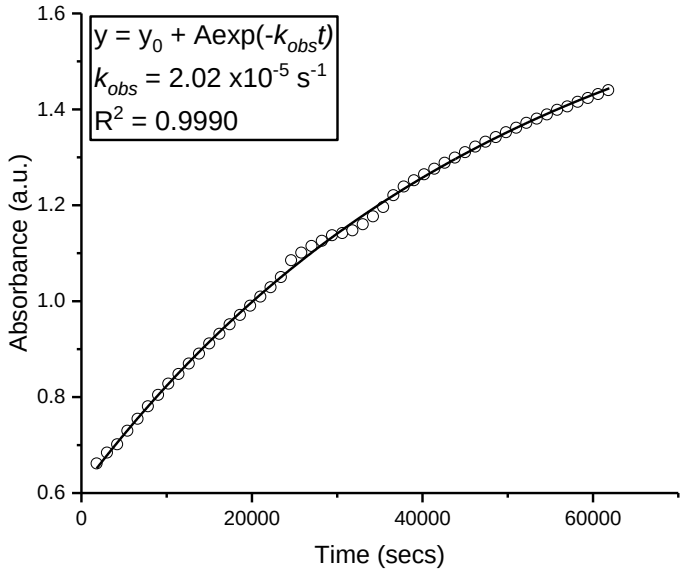

*Figure S46 – ATR-IR spectroscopy plot showing the change in absorbance vs. time plot for the 1239-1176 cm^{-1} vibrational band, during the CHO/CO_2 copolymerisation catalysed by **2e**. Reaction conditions: $[CHO]_0$ = 5 M in diethyl carbonate, $[\mathbf{2e}]_0$ = 5.6 mM, 80 °C at 1 bar CO_2 pressure. For clarity, only every 40th data point is shown.*

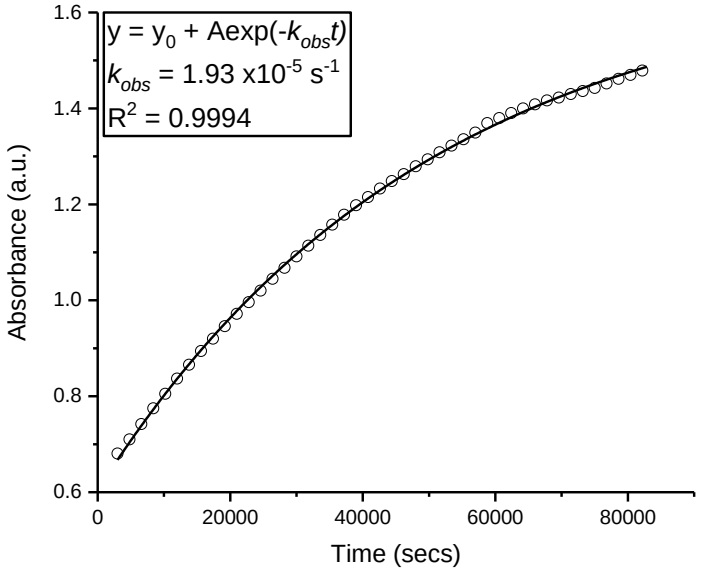

*Figure S47 – ATR-IR spectroscopy plot showing the change in absorbance vs. time plot for the 1239-1176 cm^{-1} vibrational band, during the CHO/CO_2 copolymerisation catalysed by **2e**. Reaction conditions: $[CHO]_0$ = 5 M in diethyl carbonate, $[\mathbf{2e}]_0$ = 6.33 mM, 80 °C at 1 bar CO_2 pressure. For clarity, only every 40th data point is shown.*

Raw Data for Figure 1c

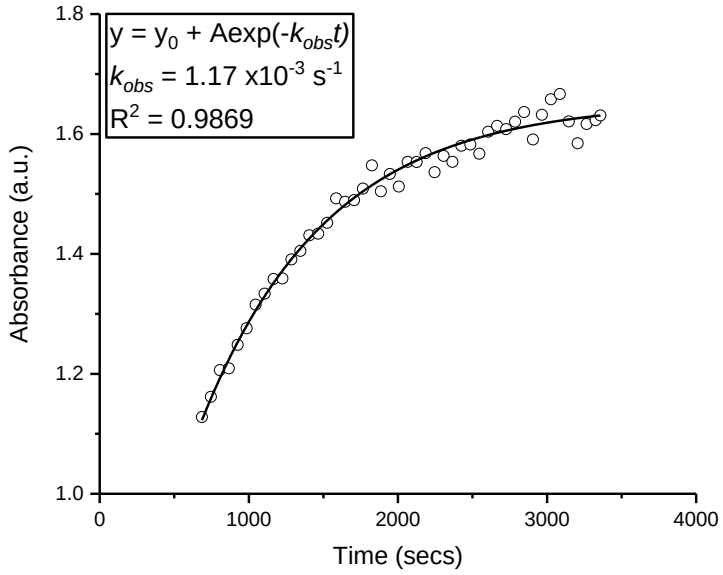

*Figure S48 – ATR-IR spectroscopy plot showing the change in absorbance vs. time plot for the 1239-1176 cm^{-1} vibrational band, during the CHO/CO_2 copolymerisation catalysed by **2e**. Reaction conditions: $[CHO]_0$ = 5 M in diethyl carbonate, $[\mathbf{2e}]_0$ = 5 mM, 120 °C at 5 bar CO_2 pressure. For clarity, only every 2nd data point is shown.*

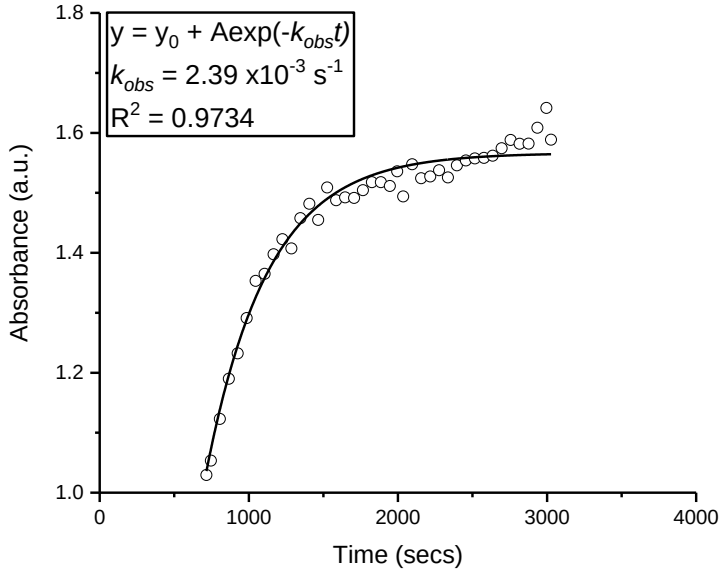

*Figure S49 – ATR-IR spectroscopy plot showing the change in absorbance vs. time plot for the 1239-1176 cm^{-1} vibrational band, during the CHO/CO_2 copolymerisation catalysed by **2e**. Reaction conditions: $[CHO]_0$ = 5 M in diethyl carbonate, $[\mathbf{2e}]_0$ = 5 mM, 120 °C at 10 bar CO_2 pressure. For clarity, only every 2nd data point is shown.*

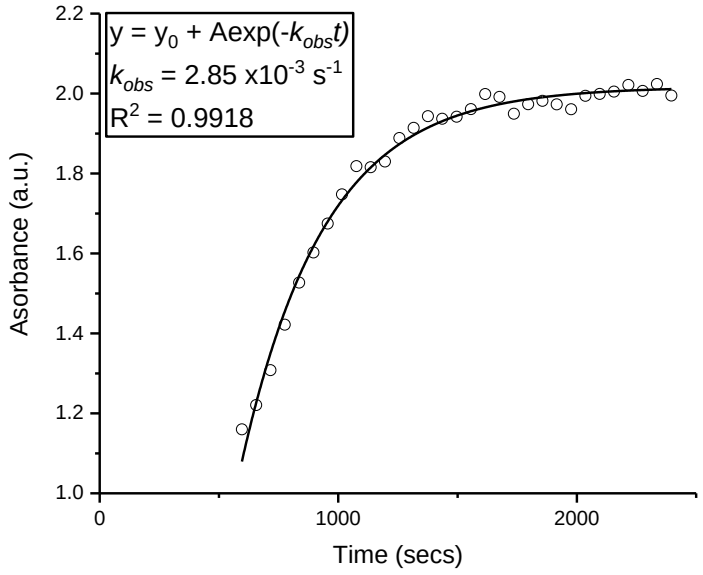

*Figure S50 – ATR-IR spectroscopy plot showing the change in absorbance vs. time plot for the 1239-1176 cm^{-1} vibrational band, during the CHO/CO_2 copolymerisation catalysed by **2e**. Reaction conditions: [CHO]$_0$ = 5 M in diethyl carbonate, [**2e**]$_0$ = 5 mM, 120 °C at 20 bar CO_2 pressure. For clarity, only every 2nd data point is shown.*

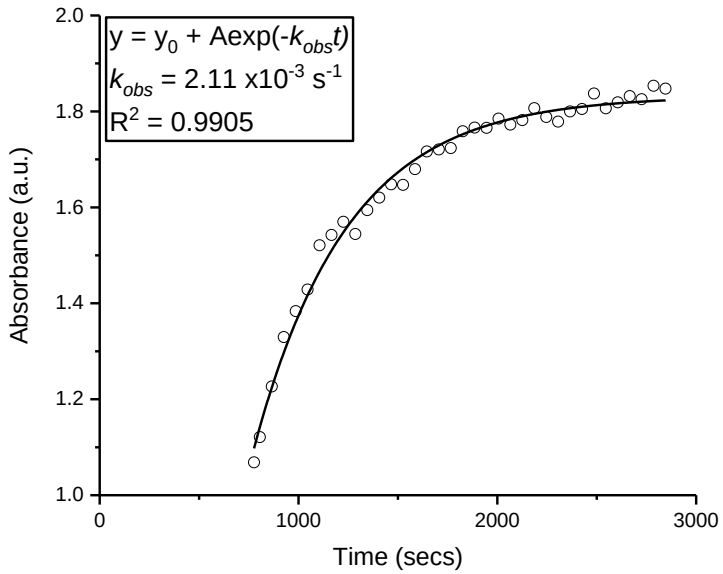

*Figure S51 – ATR-IR spectroscopy plot showing the change in absorbance vs. time plot for the 1239-1176 cm^{-1} vibrational band, during the CHO/CO_2 copolymerisation catalysed by **2e**. Reaction conditions: [CHO]$_0$ = 5 M in diethyl carbonate, [**2e**]$_0$ = 5 mM, 120 °C at 30 bar CO_2 pressure. For clarity, only every 2nd data point is shown.*

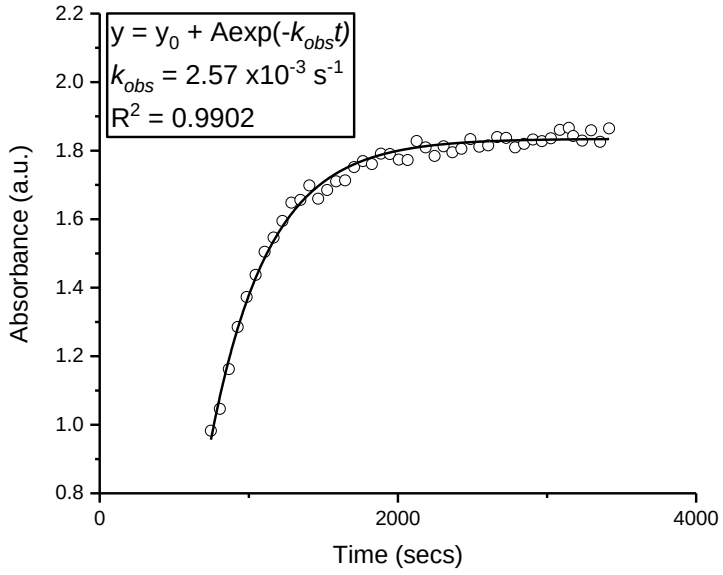

*Figure S52 – ATR-IR spectroscopy plot showing the change in absorbance vs. time plot for the 1239-1176 cm^{-1} vibrational band, during the CHO/CO_2 copolymerisation catalysed by **2e**. Reaction conditions: [CHO]$_0$ = 5 M in diethyl carbonate, [**2e**]$_0$ = 5 mM, 120 °C at 40 bar CO_2 pressure. For clarity, only every 2nd data point is shown.*

Polymerisation Kinetics of 1

The rate law using catalyst **1** was also determined and found to be the same as for **2e**. The determination of its rate law was important because: 1) it provides further support for the rate law observed for catalyst **2e** and 2) it confirms that the change in initiating group does not appear to influence the overall rate law.

Order in Epoxide

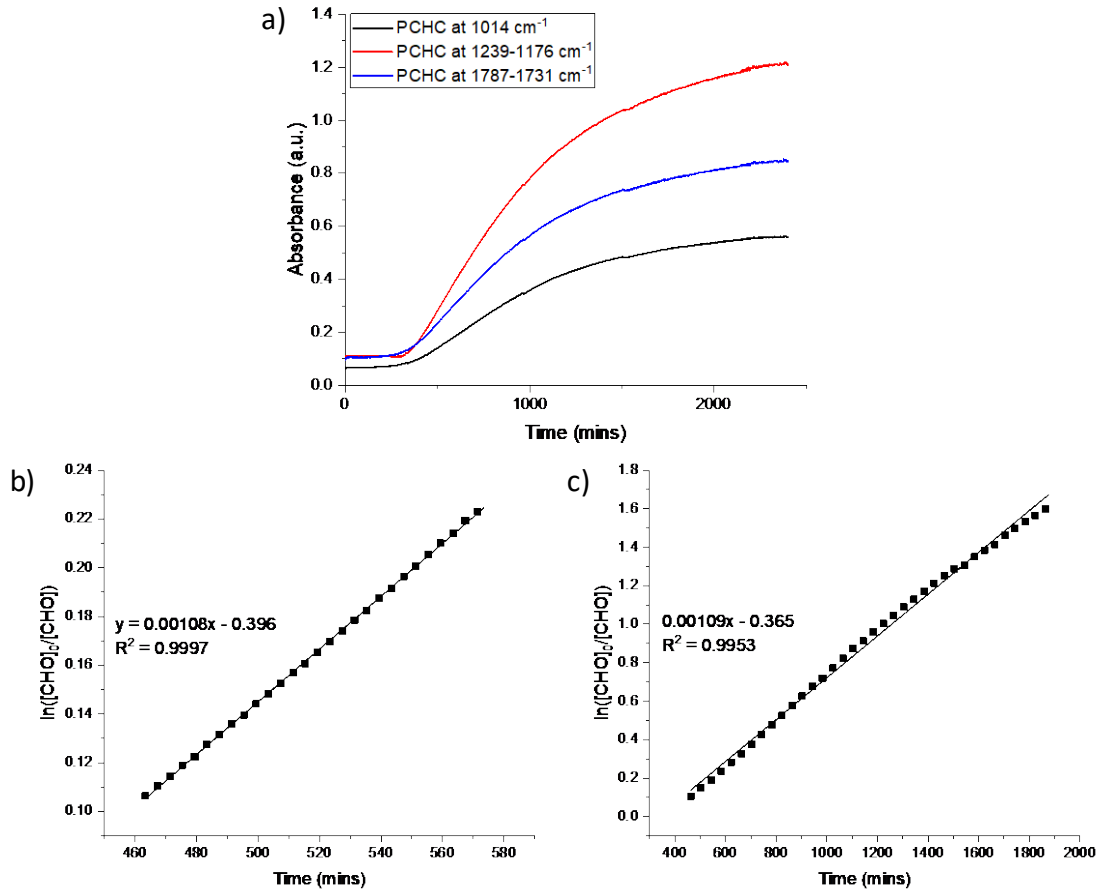

*Figure S53 – a) ATR-IR spectroscopic trace of the copolymerisation of CHO and CO_2. Reaction conditions: [**1**] = 5 mM and $[CHO]_0$ = 5 M in toluene, 80 °C, 1 bar pressure of CO_2. b) Plot of ln($[CHO_0]$/[CHO]) vs time for 10 to 20 % conversion of CHO. For clarity, every 2nd data point is shown. c) Plot of ln($[CHO_0]$/[CHO]) vs time for 10 to 80 % conversion of CHO. For clarity, every 20th data point is shown.*

Order in Catalyst

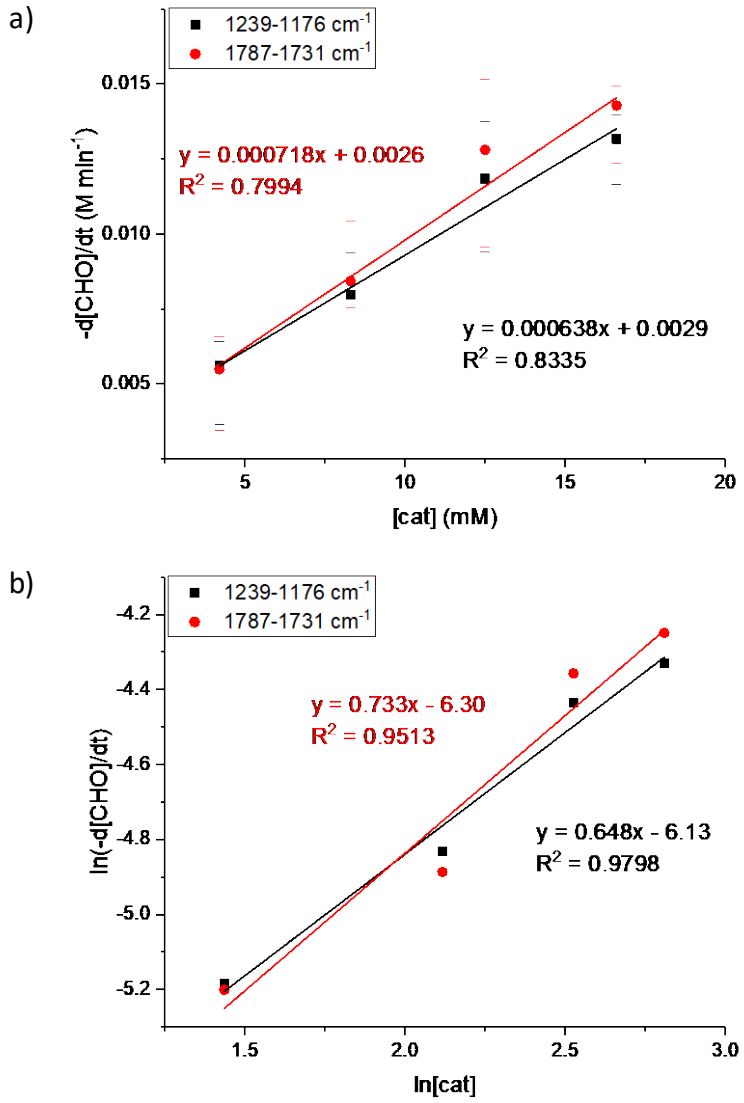

Figure S54 – Plots to determine the order in **1**. Reaction conditions: [CHO] = 8.24 M in DEC, 80 °C, 1 bar pressure CO_2. a) Initial rate of reaction (10-20 % CHO conversion) against catalyst concentration. b) A ln(initial rate) against ln(catalyst concentration) plot of the median data points measured.

Order in CO_2

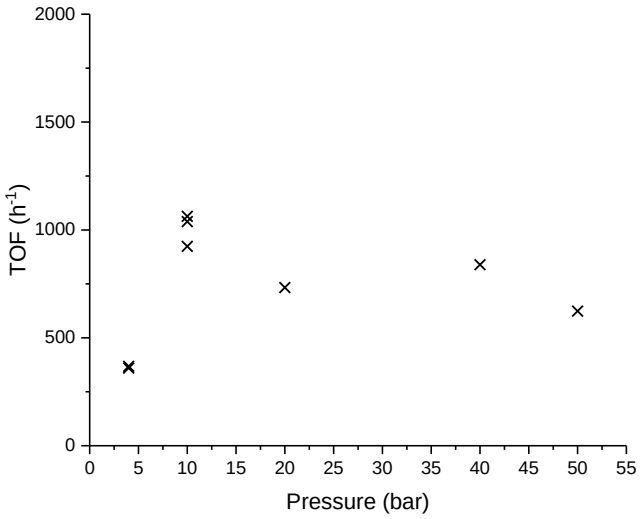

*Figure S55 – Plot of activity (TOF) against pressure for catalyst **1**. Reaction conditions: 120 °C, 5 h, 1:10,000 catalyst:CHO. Value at 50 bar from Garden et al.[3]*

8. Influence of Polymerisation Conditions

Table S3- Data showing influence of polymerisation conditions.

Cat.	Catalyst mol%	Time (h)	Temp (°C)	Pressure (bar)	PCHC (%)	TON	TOF (h^{-1})	M_n [Đ]
2b	0.1	1	120	1	96	377	435	12280 [1.04] 5340 [1.13]
2c	0.1	1	120	1	93	419	466	14490 [1.06] 5930 [1.15]
2e	0.1	0.75	120	1	> 99	430	645	21760 [1.04] 9090 [1.15]
2c	0.01	0.5	120	20	> 99	4415	8830	44400 [1.04] 21200 [1.05]
2c	0.005	4	120	20	> 99	5435	1359	54380 [1.04] 26550 [1.04]

SEC Data (Table 2)

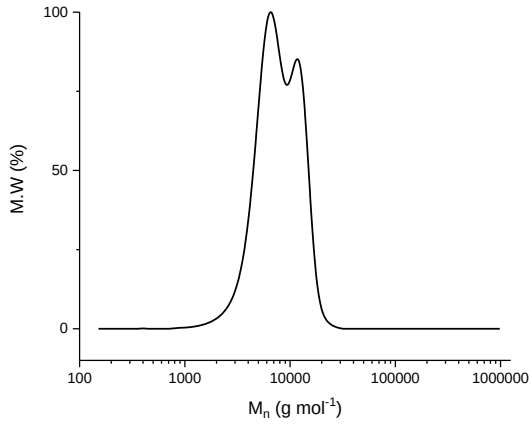

*Figure S56 – SEC plot of M_n for catalyst **2b** at 120 °C under 1 bar CO_2 for 1 hour.*

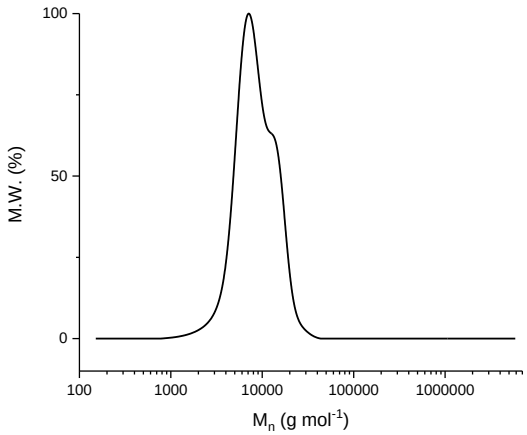

*Figure S57 – SEC plot of M_n for catalyst **2c** at 120 °C under 1 bar CO_2 for 1 hour.*

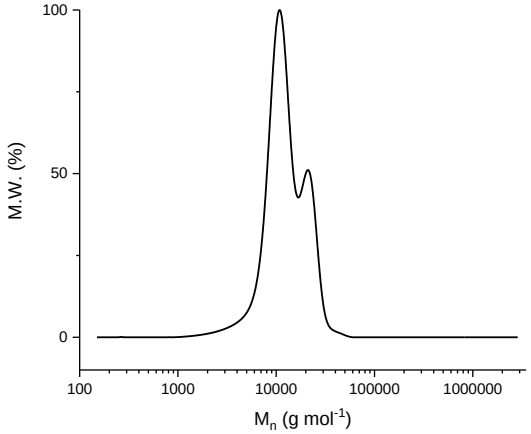

*Figure S58 – SEC plot of M_n for catalyst **2e** at 120 °C under 1 bar CO_2 for 0.75 hours.*

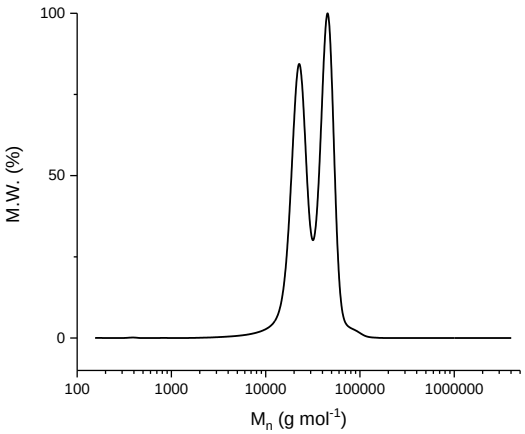

*Figure S59 – SEC plot of M_n for catalyst **2c** at 120 °C under 20 bar CO_2 for 0.5 hours at 0.01 mol% catalyst loading.*

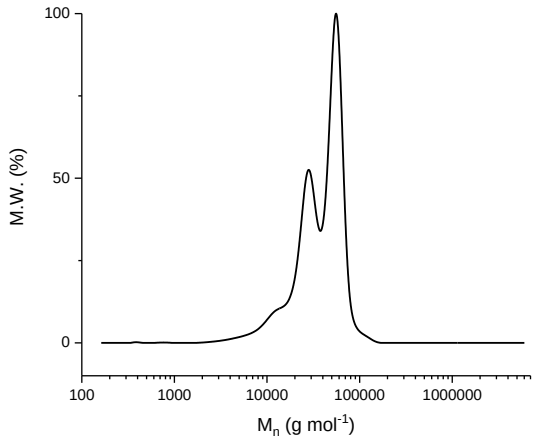

*Figure S60 – SEC plot of M_n for catalyst **2c** at 120 °C under 20 bar CO_2 for 4 hours at 0.005 mol% catalyst loading.*

9. Polymerisation Control Studies

SEC Data (Table 3)

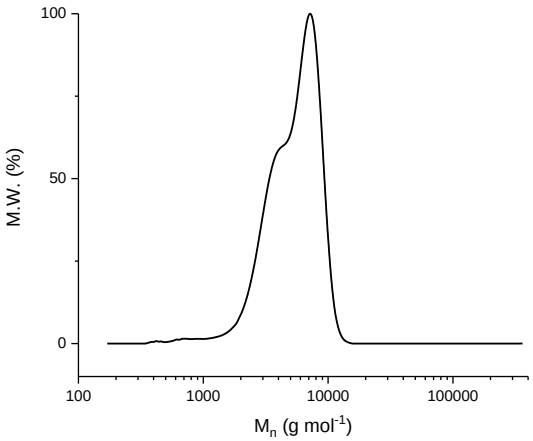

*Figure S61 – SEC plot of M_n for catalyst **2c** at 80 °C under 1 bar CO_2 for 6 hours with no added chain transfer.*

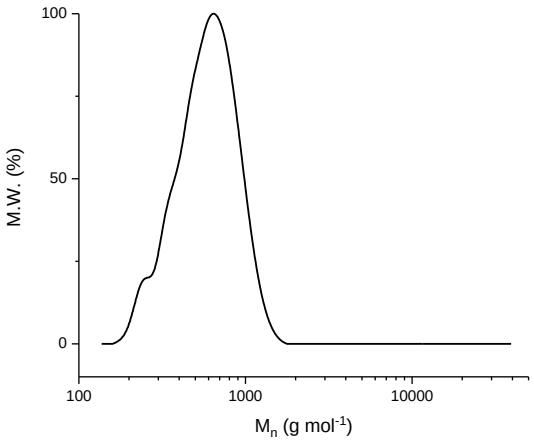

*Figure S62 – SEC plot of M_n for catalyst **2c** at 80 °C under 1 bar CO_2 for 6 hours with 10 equivalents of H_2O.*

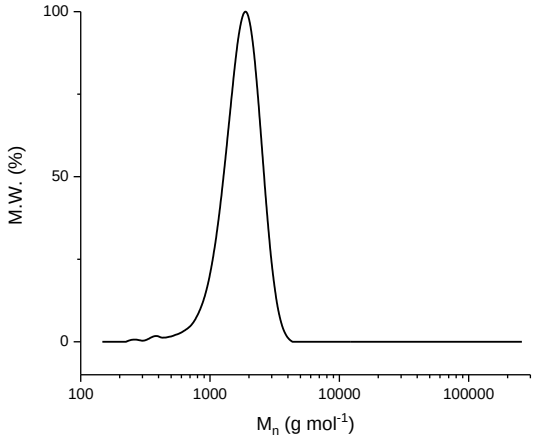

*Figure S63 – SEC plot of M_n for catalyst **2c** at 80 °C under 1 bar CO_2 for 6 hours with 10 equivalents of CHD.*

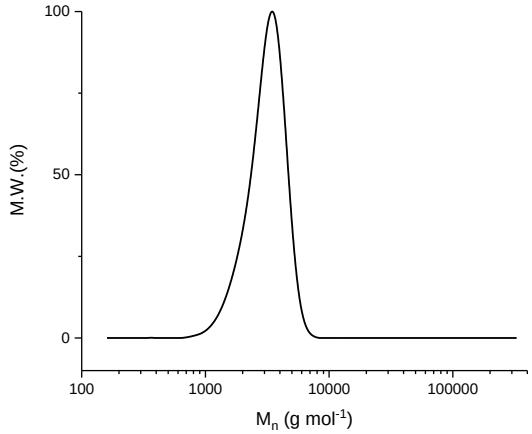

*Figure S64 – SEC plot of M_n for catalyst **2b** at 80 °C under 1 bar CO_2 for 6 hours with pre-stirring in air for 1 h.*

SEC Data (Figure 3b)

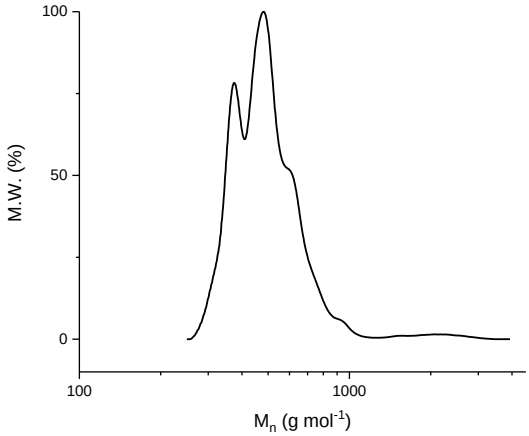

*Figure S65 – SEC plot of M_n for catalyst **2b** under 1 bar CO_2. Reaction conditions: **2b**/CHO/CHD = 1/1000/10, 80 °C, 5M in toluene. Conversion = 1.5 %.*

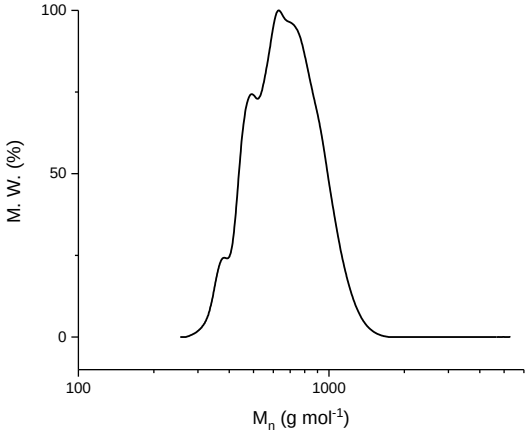

*Figure S66 – SEC plot of M_n for catalyst **2b** under 1 bar CO_2. Reaction conditions: **2b**/CHO/CHD = 1/1000/10, 80 °C, 5M in toluene. Conversion = 7.0 %.*

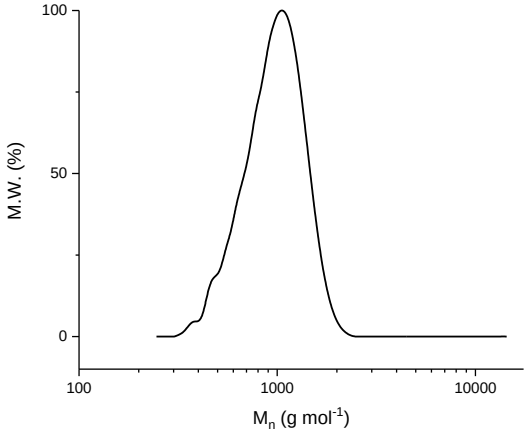

*Figure S67 – SEC plot of M_n for catalyst **2b** under 1 bar CO_2. Reaction conditions: **2b**/CHO/CHD = 1/1000/10, 80 °C, 5M in toluene. Conversion = 14.8 %.*

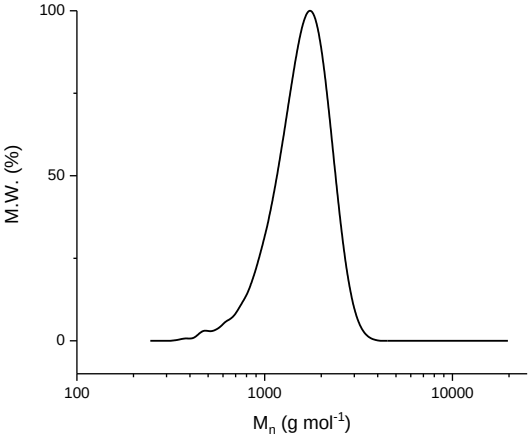

*Figure S68 – SEC plot of M_n for catalyst **2b** under 1 bar CO_2. Reaction conditions: **2b**/CHO/CHD = 1/1000/10, 80 °C, 5M in toluene. Conversion = 33.3 %.*

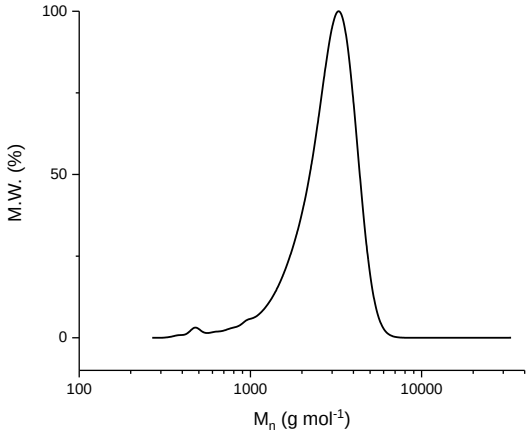

*Figure S69 – SEC plot of M_n for catalyst **2b** under 1 bar CO_2. Reaction conditions: **2b**/CHO/CHD = 1/1000/10, 80 °C, 5M in toluene. Conversion = 74.8 %.*

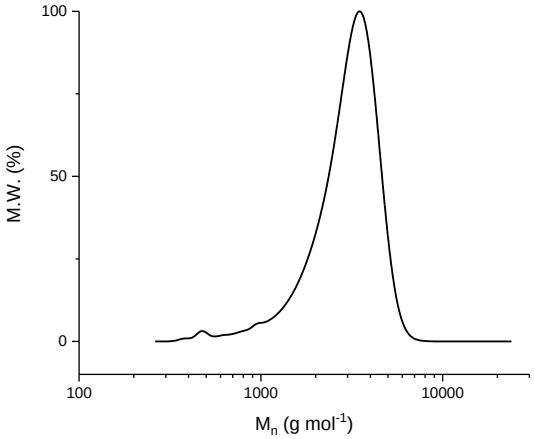

*Figure S70 – SEC plot of M_n for catalyst **2b** under 1 bar CO_2. Reaction conditions: **2b**/CHO/CHD = 1/1000/10, 80 °C, 5M in toluene. Conversion = 78.8 %.*

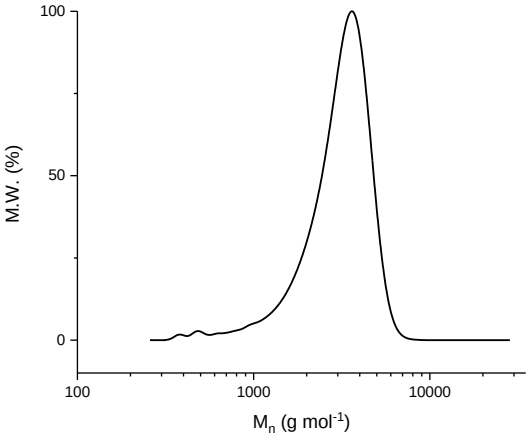

*Figure S71 – SEC plot of M_n for catalyst **2b** under 1 bar CO_2. Reaction conditions: **2b**/CHO/CHD = 1/1000/10, 80 °C, 5M in toluene. Conversion = 85.0 %.*

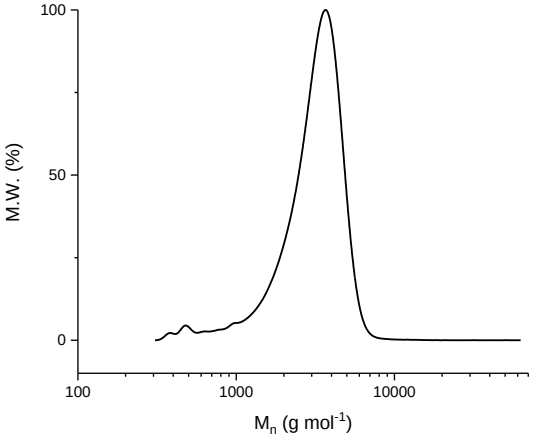

*Figure S72 – SEC plot of M_n for catalyst **2b** under 1 bar CO_2. Reaction conditions: **2b**/CHO/CHD = 1/1000/10, 80 °C, 5M in toluene. Conversion = 90.5 %.*

10. DFT Calculations

DFT calculations were performed using Gaussian 09W and applied the ωB97XD density functional and 6-31G(d) basis set, selected because it performed best in a previous comparison of different functionals.[4] The self-consistent-reaction-cavity continuum solvation model was used, with dichloromethane solvent, to model solvation in cyclohexene oxide. All transition states were characterised by normal coordinate analysis revealing precisely one imaginary mode corresponding to the intended reaction. The pathway for catalyst **[LZn$_2$(OAc)$_2$]** was already detailed by Buchard *et al*. and, to be better aligned with experimental conditions used in this work, was recalculated at 353.15 K (black pathway, Figure S73).[4] The energy levels for the propagation pathway of the dinuclear magnesium catalyst, **[LMg$_2$(OAc)$_2$]**, were also calculated (blue pathway, Figure S73). Due to the complexes' asymmetry, calculations for the heterodinuclear catalyst, **[LZnMg(OAc)$_2$]**, were conducted for both possible metal iterations. These include one calculation where the magnesium centre binds the epoxide, with the zinc alkoxide undergoing CO_2 insertion (green pathway, S73), and the other where zinc binds the epoxide and magnesium alkoxide inserts a CO_2 molecule (red pathway, S73).

Intermediate ***1*** represents the start of the propagation cycle and its energy is used to calculate the relative energies shown for all other intermediates. M_1 is defined by the starting metal-carbonate bond in intermediate ***1***. M_2 is then defined by the binding of a CHO molecule in intermediate ***2***. The rate determining step for all metal combinations is the ring-opening of the epoxide to form the transition state ***3TS***. After epoxide ring-opening, a metal alkoxide forms on M_2, with M_1 coordinating to a carbonyl on the propagating species. This coordination must be broken to insert CO_2, hence the formation of intermediate ***5***. CO_2 insertion is achieved by a series of processes where CO_2 is weakly coordinated before a zwitterionic intermediate is formed, resulting in the reformation of a metal-carboxylate on M_1 in intermediate ***10***. Intermediate ***11*** is the final calculation shown, and the start of the second propagation cycle, in an analogous conformation to intermediate ***1*** where the propagating chain is non-coordinating and the catalyst primed for epoxide binding.

No obvious qualitative differences were observed in the mechanisms for the catalysts. The computationally derived rate determining step is the ring-opening of the epoxide in all cases, with smaller transition energies for the insertion of CO_2. This is consistent with the rate equation derived experimentally. Analogous intermediates and transition states for **[LZnMg(OAc)$_2$]** and **[LMg$_2$(OAc)$_2$]** were observed for all stages of the propagation pathway previously found for **[LZn$_2$(OAc)$_2$]**, suggesting that the most likely pathway for the heterodinuclear complexes is the chain-shuttling mechanism. The calculations suggest that epoxide binding (***2***-***1***, S73) is energetically most favourable when M_2 is a magnesium centre (blue and green). The energy barrier for CO_2 insertion appears lower (***7TS***-***4***, S73) when M_1 is a zinc centre (black and green). This would imply that a catalyst combining these two features (i.e. **[LZnMg(OAc)$_2$]** in the green regime), would have a significantly lower activation energy for the copolymerisation. However, the putative rate limiting step energy barrier (***3TS***-***2***, S73) is similar for all four combinations. For catalyst **[LZnMg(OAc)$_2$]** $\Delta G^{\dagger}_{3TS}$ is equal to +24.2 (red) or +23.9 (green) kcal·mol^{-1}. Catalyst **[LMg$_2$(OAc)$_2$]** has a $\Delta G^{\dagger}_{3TS}$ of +25.4 and **[LZn$_2$(OAc)$_2$]** a $\Delta G^{\dagger}_{3TS}$ of +23.0 kcal·mol^{-1}. These energy differences are likely to be within error of the calculations and so meaningful comparisons cannot be drawn.

Fig. S73: Illustrates the DFT calculated pathways for alternating copolymerisation using a di-zinc (black), di-magnesium (blue) and heterodinuclear catalyst (red or green).

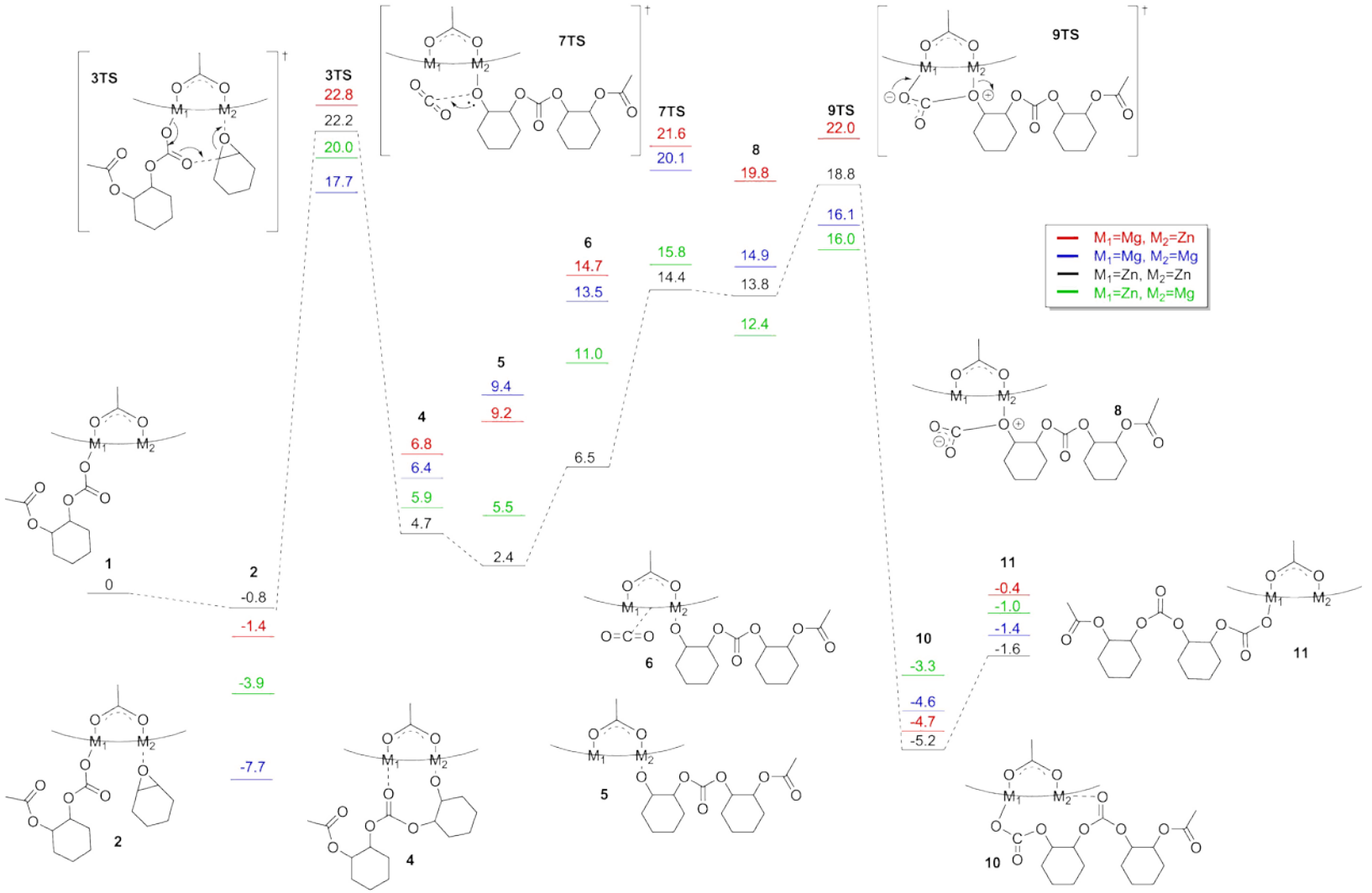

11. References

1. M. R. Kember, P. D. Knight, P. T. R. Reung and C. K. Williams, *Angew. Chem. Int. Ed.*, 2009, **48**, 931-933.
2. L. J. Gooßen, N. Rodríguez, P. P. Lange and C. Linder, *Angew. Chem. Int. Ed.*, 2010, **49**, 1111-1114.
3. J. A. Garden, P. K. Saini and C. K. Williams, *J. Am. Chem. Soc.*, 2015, **137**, 15078-15081.
4. A. Buchard, F. Jutz, M. R. Kember, A. J. P. White, H. S. Rzepa and C. K. Williams, *Macromolecules*, 2012, **45**, 6781-6795.